

Molecular Assembly on Two-Dimensional Materials

Avijit Kumar,^{1*} Kaustuv Banerjee,¹ Peter Liljeroth¹

¹Department of Applied Physics

Aalto University School of Science, P.O. Box 15100, 00076 Aalto, Finland

*To whom correspondence should be addressed; E-mail: avijit.kumar@aalto.fi.

Molecular self-assembly is a well-known technique to create highly functional nanostructures on surfaces. Self-assembly on two-dimensional materials is a developing field driven by the interest in functionalization of 2D materials in order to tune their electronic properties. This has resulted in the discovery of several rich and interesting phenomena. Here, we review this progress with an emphasis on the electronic properties of the adsorbates and the substrate in well-defined systems, as unveiled by scanning tunneling microscopy (STM). The review covers three aspects of the self-assembly. The first one focuses on non-covalent self-assembly dealing with site-selectivity due to inherent moiré pattern present on 2D materials deposited on substrates. We also see that modification of intermolecular interactions and molecule-substrate interactions influences the assembly drastically and that 2D materials can also be used as a platform to carry out covalent and metal-coordinated assembly. The second part deals with the electronic properties of molecules adsorbed on 2D materials. By virtue of being inert and possessing low density of states near the Fermi level, 2D materials decouple molecules electronically from the underlying metal substrate and allow high-resolution spectroscopy and imaging of molecular orbitals. The moiré pattern on the 2D materials causes site-selective gating and charging of molecules in some cases. The last section covers the effects of self-assembled, acceptor and donor type, organic molecules on the electronic properties of graphene as revealed by spectroscopy and electrical transport measurements. Non-covalent functionalization of 2D materials has already been applied for their application as catalysts and sensors. With the current surge of activity on building van der Waals heterostructures from atomically thin crystals, molecular self-assembly has the potential to add an extra level of flexibility and functionality for applications ranging from flexible electronics and OLEDs to novel electronic devices and spintronics.

1 Introduction

Molecular self-assembly on solid surfaces have been studied with an aim to create ultra-high density functional nanostructures which can be fabricated in a parallel fashion. Structure of such assembly is driven by the interplay of the intermolecular and molecule-substrate interactions. On weakly interacting surfaces, molecules typically interact with substrate only through van der Waals (vdW) interactions; the structure of the assembly is then determined by intermolecular forces. For example, van der Waals forces result in close-packed assemblies where the symmetry is determined by the geometry of adsorbed molecules [1], while slightly stronger and directional interactions (*e.g.* hydrogen, metal-coordination or covalent bonds) lead to structures with more varied and open assembling motifs [2,3]. This simple picture changes on interacting substrates, where the surface is not an innocent bystander [4]. In extreme cases, native metal adatoms can be incorporated into the network [5] or adsorbate induced reconstruction of the surface can lead to new self-assemblies [6,7]. Furthermore, the reactive d_z orbitals of the metal often interact quite strongly with the molecules, adding an extra factor in the assembly process and changing the properties of the molecules compared to those in the gas phase.

Molecular self-assemblies can be fundamentally different in the case of two-dimensional (2D) materials, such as graphene, hexagonal boron nitride (hBN), and transition metal dichalcogenides (TMDCs), which have attracted enormous interest recently [8–10]. The study of atomically thin crystals has been initially dominated by research on graphene. Graphene consists of sp^2 hybridized carbon atoms in a triangular lattice with a two-atom unit cell. The out-of-plane p_z orbitals form delocalized bonding π and antibonding π^* bands. These bands touch at the K - and K' -points of the Brillouin zone (also known as the Dirac points) resulting in a linear dispersion of the charge carriers that renders graphene a zero band gap semimetal [11]. The rise of graphene has been closely followed by that of monolayer hBN. It is isostructural to graphene, with boron and nitrogen, instead of carbon, forming the basis of a similar triangular lattice (the lattice parameters of graphene and hBN differ by 1.8%) [12]. Unlike graphene, hBN is an insulator with a band gap of ~ 6 eV. Monolayers of TMDCs are the latest entrant to the family of 2D crystals and a lot of work is going on to unravel the unique properties of these atomically thin materials [13]. Although the spectrum of 2D material is expanding rapidly [14], the study of molecular self-assembly has so far, to a large degree, been concentrated on graphene and hBN only.

Investigation of adsorbed single molecules and assemblies on 2D materials is important for several reasons. Essentially all of the atoms on these materials are on the surface; hence, covalent or even non-covalent functionalization can completely change their physical and electronic properties [15]. This has already been shown for graphene where covalent functionalization using hydrogen, oxygen, or fluorine has modified the electronic properties with the functionalized carbon atoms being rehybridized from sp^2 to sp^3 [16–18]. Non-covalent functionalization using molecular adlayers has been suggested as means of tailoring graphene’s band structure without compromising its excellent electronic properties, boosting its potential applications in electronics or sensors. This implies that the study of molecular assembly on graphene is most relevant on technologically important, insulating substrates *e.g.*, silicon dioxide (SiO_2) or bulk hBN for real device applications. Also at very nascent stage of research, chemical functionalization of TMDCs have shown to alter their electronic properties [19]. In general, chemical functionalization can be used to engineer 2D materials in devices through formation of surface dipoles, charge transfer, energy band alignment, and orbital interactions. Molecular adlayers can help enable novel applications that are only made possible through the unique properties of 2D materials.

Secondly, both graphene and hBN offer inert surfaces on which the fundamental principles of surface assembly can be verified. Close-packed molecular assemblies with weak intermolecular bonds or hydrogen-bonded networks have been studied extensively on graphene - reviews of such studies can be found in Refs. [20,21]. An important point here is that the bulk substrate supporting the atomically thin 2D material can have a significant effect on the molecular assembly. As we discuss in Sec. 2, the structural and electronic landscape of both epitaxial graphene and hBN is intimately dependent on the surface on which it is grown. Periodic structural, as well as electronic corrugation, on these surfaces can lead to highly site-selective molecular adsorption - examples will be given in Sec. 3.1. Sec. 3.2 describes close-packed assembly on epitaxial graphene while Sec. 3.3 offers engineering aspects of assembly on 2D materials. The first layer of molecular network has often been used to form templates for multi-component, hierarchical growth of molecules - these phenomena will be discussed in Sec. 3.4. Studies on chemical reactions of molecules on graphene and hBN will be reviewed in Sec. 3.5.

Furthermore, due to their inertness, graphene and hBN can be used as ultrathin decoupling layers. Low-temperature scanning tunneling microscopy (STM) studies make it possible to resolve intramolecular features; increased lifetime of injected electrons results in narrow spectral features and make it possible to visualize molecular orbitals in real space. In Sec. 4, the rich field of using graphene and hBN as substrates in the study of single-molecules will be explored. Sec. 4.1 illustrates orbital imaging of molecules on 2D materials. On strongly site-selective assemblies, the electronic properties of the molecules are modulated according to the potential landscape of the underlying 2D material as will be shown in Sec. 4.2. In some cases, the electric field from the STM tip can lead to charging of the molecule (gating) on the surface, this effect has been illustrated in Sec. 4.3.

After the discussion on molecular self-assembly on epitaxial layers of 2D materials, we turn to the technologically more relevant systems where the 2D-material has been deposited on insulating substrates. Some examples of direct, scanning-probe observation of molecular self-assembly on such substrates will be summarized in Sec. 3.2. The effect of molecular layers on the electronic properties of graphene on such samples has been studied using photoelectron spectroscopy (PES), Raman spectroscopy, and current-voltage ($I - V$) measurements on graphene field-effect transistors (FETs). These results will be summarized in Sec. 5.

This review is limited to the studies of ordered adlayers of molecules on 2D materials, primarily graphene and hBN. The emphasis is on the electronic effects of the assembled molecules (and the surface underneath) principally investigated by STM in ultra-high vacuum conditions at low temperature. For a more general review of molecular assembly on graphene readers are directed to Refs. [20,21]. Non-covalent functionalization of graphene is a vast field and has been reviewed extensively in Refs. [22–26]. Review of covalent approaches toward functionalizing graphene can be found in Refs. [16,21,27–29]. Finally, surface functionalization of TMDCs and two dimensional materials other than graphene has been reviewed in Refs. [19,30–32].

2 Two-dimensional materials

2D crystals are only one atomic layer thick and hence, for most practical purposes they have to be supported by a bulk substrate. The nature of the support and its interaction with the 2D material are important in determining the surface electronic structure and, through the molecule-substrate interactions, it also affects molecular self-assembly. Graphene, the first 2D material to be discovered, was first obtained by means of mechanical exfoliation of graphite onto silicon dioxide surface. Since then, other means of producing graphene (*e.g.*, chemical

exfoliation of graphite, chemical vapour deposition (CVD) on metals) and transferring it onto insulating substrates (*e.g.*, SiO₂, bulk hBN, polymers) have emerged [33]. In recent years, graphene (produced by exfoliation or CVD) transferred onto bulk hBN has attracted a lot of attention as many properties of free-standing graphene are retained on hBN and it has emerged as the *de facto* standard substrate in the highest performance graphene devices [34,35]. The atomically smooth surface of graphene on hBN presents the ideal surface on which molecular self-assembly on graphene can be tested. However, the transfer processes involved can result in contamination on the graphene surface, which naturally hinders precise studies of molecular self-assembly.

Graphene for studies on molecular self-assembly in well-defined and controlled environment (ultra-high vacuum, UHV) is mostly obtained *in situ* via epitaxial growth on single crystals. Graphene can be grown by thermal sublimation of silicon from silicon carbide (6H-SiC(0001)) crystals [36] or by thermal decomposition of hydrocarbons on the hexagonal surfaces (FCC(111) or HCP(0001)) of transition metal single crystals [37]. Recently, some methods for the direct growth of graphene on insulating substrates have also been presented [38]. The substrate can have a significant effect on properties of the epitaxial graphene layer and the substrates can be classified into weakly and strongly interacting ones. Single layer graphene grown on SiC (G/SiC) is weakly coupled to the substrate with the graphene-substrate distance (3.3 Å) [39] being close to the inter-layer separation in graphite. This indicates that the graphene interacts with the substrate only through van der Waals forces, which is reflected in the electronic properties being close to those of free-standing graphene [40]. On the other hand, the interaction of graphene grown on metals depends on the substrate and has been discussed in detail in Refs. [37, 41]. Graphene-metal systems with a lattice mismatch gives rise to a long-range, periodic superstructure called the moiré pattern. The geometry and electronic properties of graphene vary over the moiré unit cell due to the periodically modulated carbon adsorption site w.r.t. the metal substrate. In the regions where the center of the carbon ring sits on top of the surface metal atom, the carbon-metal interaction is typically weak - at these points (so-called TOP-site) the graphene sheet is the farthest away from the metal surface. On the other hand, when alternate carbon atoms are positioned over the surface metal atoms, strong interaction between them leads to a lower adsorption height of the graphene sheet (valley site). In the low lying areas of the moiré further differentiation can be made on the basis of whether the carbon atoms not on top of metal atoms are on the FCC-hollow site (FCC-site), the HCP-hollow site (HCP-site), or in between these sites (bridge site) of the surface metal atoms. This is shown in Fig. 1a. Within the limit of this periodic variation, if the mean graphene-metal distance (Δ_{avg}) is large, as in the case of graphene on iridium (G/Ir(111) ~ 3.4 Å) or platinum (G/Pt(111) ~ 3.3 Å), the resulting system is a weakly interacting [42–45]. In these systems the topographic corrugation (Δ_{corr}) over the moiré unit cell is small (< 0.5 Å) and graphene retains its linear dispersion. Conversely, graphene grown on ruthenium (G/Ru(0001)) or rhodium (G/Rh(111)) interact strongly with the metal, and the graphene-metal distance varies from ~ 2.1 Å in the bridge sites (significant carbon-metal hybridization) to > 3.6 Å at the TOP sites (free-standing graphene) [46, 47]. This is accompanied by a variation of work-function of 0.32 eV across the moiré unit cell and has profound implications in terms of adsorption energy of molecules at the different moiré sites. The lattice matched graphene-nickel (G/Ni(111)) system which does not show any superstructure because of 1×1 commensurate growth is another example of strongly interacting graphene [48–50]. The electronic properties of graphene on strongly interacting metals are strongly modified, including the possible opening of a band-gap [51].

Epitaxial growth of hBN behaves in many ways similarly to that of graphene. The most widely used way to obtain hBN is by thermal decomposition of borazine (B₃H₆N₃) on transition

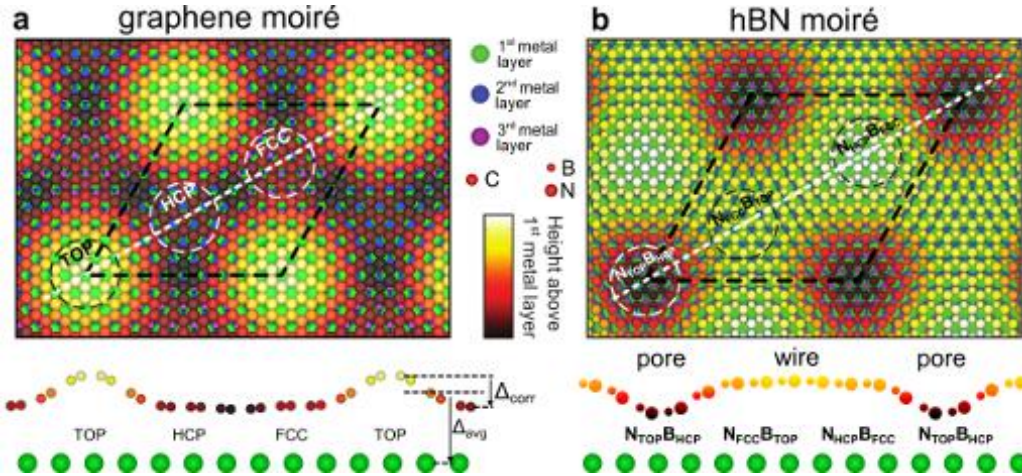


Figure 1: **2D epitaxial substrates.** (a) A schematic of a moiré pattern in graphene due to lattice mismatch between graphene and the underlying substrate. The lower panel shows a corrugation profile of the moiré along the white line. (b) A schematic of moiré pattern in hBN due to lattice mismatch between hBN and the underlying substrate. The lower panel depicts corrugation profile along the white line across the moiré. Adapted with permission from [45,52].

metals; the surface properties of hBN are again dictated by the metal underneath [53]. Here too, lattice mismatch between the hBN and the metal substrate leads to moiré pattern as shown in Fig. 1b. In hBN-metal systems the region of strong interaction is limited to the sites where the N-atoms are on the top of the metal surface atoms. For other adsorption sites of the B and N atoms (*i.e.*, TOP-FCC or HCP-FCC) the hBN-metal interaction is weak. Thus, the moiré of hBN on metals is characterized by periodically arranged, interacting “pore” areas separated by connected regions of almost free-standing “wires”. The terminology of pores and wires stems from historical reasons [54]; nevertheless, the hBN layer forms a full, atomically perfect layer without holes or other defects. The moiré topography is in contrast to graphene where connected valley sites separate isolated, periodic TOP sites [55] (compare Fig. 1a to Fig. 1b). The corrugation of the hBN “nanomesh” varies from metal to metal. If the mean hBN-metal distance is comparable to inter-layer distance in bulk boron-nitride (~ 3.33 Å) as in the case of epitaxial hBN on Ir(111), Pt(111), or Cu(111), the topographic corrugation is small (*e.g.*, ~ 0.35 Å for hBN/Ir) [52, 56, 57]. For hBN grown on Ru(0001) or Rh(111) the minimum hBN-metal height is low (~ 2.5 Å) and the resulting corrugation is quite high (~ 1 Å) [58, 59]. Irrespective of the supporting bulk metal, hBN shows a high electronic corrugation over the period of the moiré resulting in a significant difference in the local work-function between the wire and pore sites (~ 0.5 eV for hBN on Rh, Ru or, Ir and, ~ 0.3 eV for hBN/Cu) [53].

While the bulk support can have an effect on the properties of graphene and hBN, they are otherwise chemically relatively inert. Thus, molecules deposited on them interact with the 2D surface primarily through weak, van der Waals or $\pi - \pi$ interactions. This makes these surfaces quite attractive for studying the fundamentals of supramolecular self-organization. We will go through self-assembly on 2D materials in detail in the next section.

3 Molecular assembly on 2D materials

Control over the strength of the molecule-substrate interaction and its spatial variation is the key to tuning the molecular adsorption patterns. If the molecule-substrate interactions are

weaker than the intermolecular attraction, a close-packed islands of molecules will be observed also on non-smooth surfaces. On the other hand, stronger site-specific molecule-substrate interaction leads to site-selective adsorption.

3.1 Site-selective adsorption

First we will focus on the site-selective adsorption on strongly interacting G/Ru(0001) surface where the moiré pattern plays an active role in the assembly formation. Self-assembly of free-base phthalocyanine (H_2Pc) [60,61], iron phthalocyanine (FePc) [60–63], nickel phthalocyanine (NiPc) [60,61], manganese phthalocyanine (MnPc) [61], pentacene [62,64], perylene-3,4,9,10-tetracarboxylic-3,4,9,10-dianhydride (PTCDA) [65,66], tetracyanoquinodimethane (TCNQ) [67,68] and fullerene (C_{60}) [69,70] have been studied on this surface. At lower coverage, individual MPc molecules occupy FCC region of the moiré. As the molecular coverage is increased, the molecules begin to occupy edges of the TOP region instead of HCP region. For a certain coverage, this results in the formation of a Kagome lattice, where the TOP sites still remain unoccupied while the FCC and HCP sites are occupied. The coverage dependent assembly has been studied by Gao and coworkers [60,62] for FePc molecules (shown in Figure 2a-c). Other examples include H_2Pc , NiPc , FePc , MnPc molecules on G/Ru surface [60,61] which were shown to also form a Kagome lattice for right coverage.

Zhang *et al.* [62] studied molecular self-assembly of FePc and pentacene molecules on G/Ru(0001). *Ab initio* calculations suggest that the in-plane surface dipole (due to the work function modulation within the moiré unit cell) exists around the edge of the TOP region with the largest values along the TOP-FCC direction of the moiré. Therefore, molecules having significant polarizability tend to adsorb preferentially at FCC site. The enhanced stabilization of the molecules is the result of the interaction between the induced dipole moment of the molecule and the in-plane surface dipole [73]. A large electric field in FCC-TOP direction due to the surface dipole is confirmed by the fact that pentacene molecules adsorbs exclusively along this direction at low coverage [64]. Density functional theory (DFT) calculations including vdW interactions demonstrated that the adsorption energy of the molecule was highest in this configuration. Increased deposition leads to sequential filling up of all FCC positions followed by the filling of the HCP sites – the TOP regions remain unoccupied even at high coverage of 0.7 monolayer (ML). A site-dependence of the adsorption energy is also at the heart of hierarchical adsorption of C_{60} molecules on G/Ru [69]. Unlike the previously described molecules, the buckyballs start by populating the HCP valley sites to form heptamers before continuing onto the FCC sites and finally onto the TOP sites. A combination of decreasing adsorption energy and decreasing amount of charge transferred to C_{60} from HCP to the TOP sites, as indicated by DFT calculations, was suggested as a reason for the hierarchical growth.

TCNQ molecules deposited on G/Ru also show site-selective adsorption [67,68]. Here, the adsorption mechanism is different from the dipole mediated adsorption as discussed earlier. TCNQ molecules are known to be strong electron acceptors with an electron affinity of 2.8 eV [74]. Therefore, such molecules tend to adsorb at the sites with higher electron density and lower work function [67] *i.e.*, the HCP and FCC region compared to the TOP region. It is also possible that higher reactivity of the FCC/HCP sites compared to the TOP regions contributes to the patterned assembly. At slightly higher coverage all the FCC and HCP regions are covered while the TOP regions stay unoccupied creating a Kagome lattice. At full monolayer coverage the molecules occupy the TOP region as well. The coverage dependent site-selective adsorption is shown in Fig. 2d-f.

Molecular self-assemblies on epitaxial hBN layer grown on metal surfaces also exhibit site-

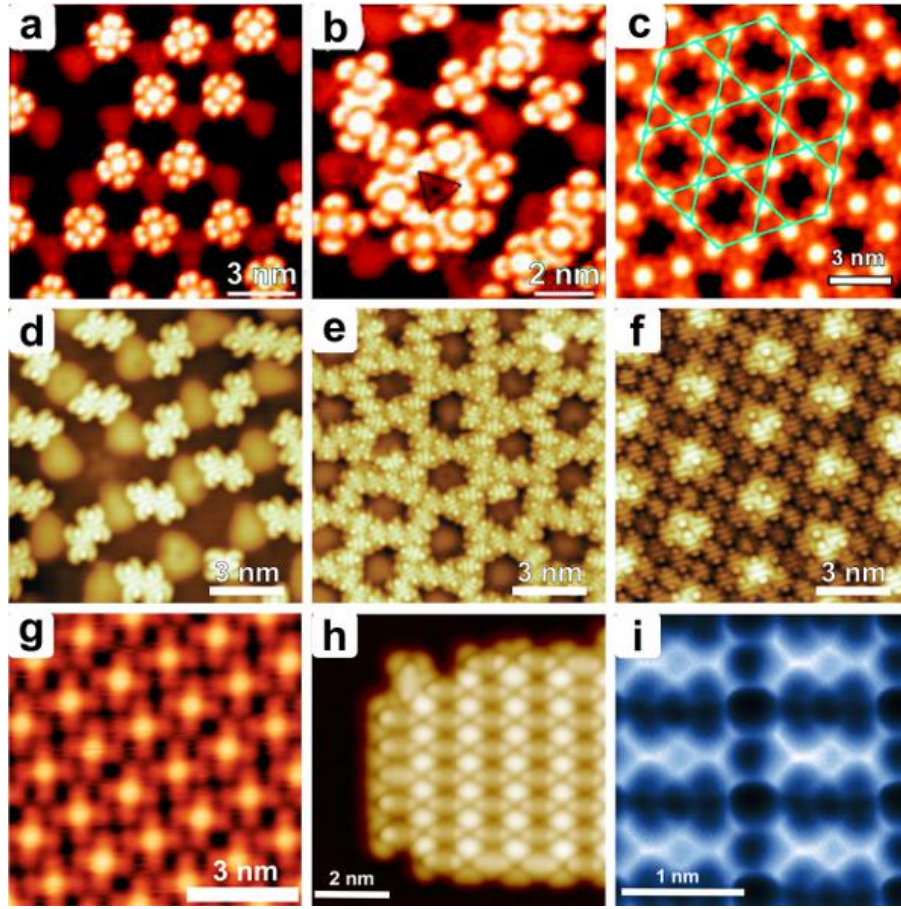


Figure 2: **Site-selective assembly on epitaxial graphene.** (a) Site-selective assembly of FePc molecules on G/Ru(0001) surface. The molecules occupy the FCC sites of the moiré. The TOP site of the moiré is brighter than the low lying area. (b) As the coverage is increased, the molecules begin to occupy the HCP sites while the TOP sites still remain occupied [62]. (c) At sufficiently high coverage, these molecules form a Kagome lattice, highlighted in the image [60]. (d) Similarly, TCNQ molecules adsorb on HCP and FCC areas at lower coverages and with increasing coverage they form (e) a Kagome lattice and for even higher coverage they form (f) a continuous monolayer [68]. (g) On the weakly interacting surface of G/Ir(111), CoPc form closed packed islands even at a sub-monolayer coverage [71]. Due to reduced screening in graphene on hBN, F_4 TCNQ assemble in a close-packed geometry at sub-monolayer coverage as evidenced by (h) STM and (i) non-contact atomic force microscope images [72]. Adapted with permission from [60, 62, 68, 71, 72].

selectivity due to the presence of a moiré pattern. The presence of a significant geometric corrugation and periodic modulation of the work function across the hBN moiré also makes it an appealing substrate for templated molecular assembly. A number of molecules such as C_{60} [54], naphthalocyanine [78], CuPc [59, 75], H_2Pc [75], CoPc [76], H_2Pc [77], 5,5',5'',5''',5''''-hexaiodocyclohexa-m-phenylene (I_6CHP) [79], and TCNQ [77] selectively adsorb on the pores of the hBN surface. Similar to the case of G/Ru, the adsorption mechanism is related to the presence of in-plane electric field due to the strong work function modulation, which results in trapping the molecules in the pores [59, 75].

In epitaxial hBN, the maximum potential gradient exists at the edge of the pore (up to 1 V/nm) causing the molecules to adsorb there (Fig. 3a,b). CoPc on hBN/Ir(111) [76] and

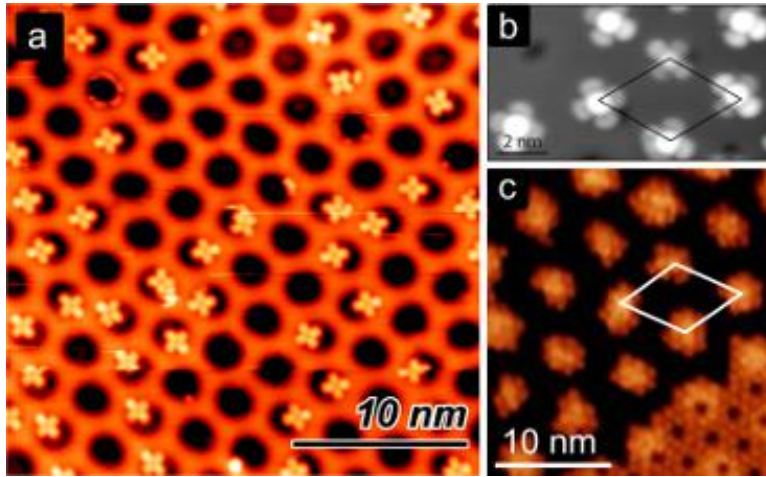


Figure 3: **Site-selective assembly on hBN.** (a) CuPc molecules adsorb preferentially on the pore site of hBN/Rh(111) nanomesh. [75] (b) CoPc molecules preferentially adsorb on the pore sites of hBN/Ir(111) moiré [76]. (c) Extended self-assembled 2H-P islands form on hBN/Cu(111) confined to certain areas of the moiré. The moiré unit cell is shown by the white rhombus. The islands can merge to form a continuous monolayer as seen in the bottom-right corner [77]. Adapted with permission from [75–77].

I₆CHP [79], H₂Pc, and CuPc on hBN/Rh(111) [75] are examples of such off-centre adsorption. Aggregates of small molecules such as porphine and TCNQ on long-period hBN moiré on Cu(111) (periodicity 12 nm) nucleate at the pore site for low coverages [77]. A similar observation has been made for Xe atoms on hBN/Rh(111) surface [59, 80].

On systems with a shorter moiré period, preferential adsorption in the pore regions disturb the long-range order of the molecular layer. For example, deposition of nearly a full-monolayer of CoPc on hBN/Ir results in short range order with a close-packed square lattice [76]. However, there is no long range order due to the strong molecule-substrate interactions in the pores of the hBN moiré on Ir(111) and the mismatch in the preferred nearest-neighbour distance in the molecular layer and the moiré period.

While free-base porphine (2H-P) exhibits site-selective adsorption on hBN/Cu(111) surface [77] as shown in the Fig. 3c, it is possible to tailor the intermolecular interactions by adding terminal groups to porphine molecules resulting in the loss of site-selectivity. Carbonitrile-functionalized porphyrin molecules (2H-TPCN) deposited on hBN/Cu(111) [81] show close-packed islands, because non-covalent intermolecular attraction (due to the presence of terminal cyano-bi-phenylene groups) dominates over the molecule-substrate interaction.

3.2 Close-packed assembly

Site-selectivity is not expected on weakly interacting systems, where the work-function modulation and the geometric corrugation across the moiré unit cell are small [82–84]. Precisely this has been observed for TCNQ [85] and MPc molecules (e.g. CoPc [71, 86], CuPc [71], and F₁₆CoPc [71]) on G/Ir(111). An example of CoPc on G/Ir(111) is shown in Fig. 2g. While the work function modulation and geometrical corrugation are too small to dictate the assembly of molecules, their unit cell can differ slightly from ideal square packing [86]. Close-packed molecular islands with the exact geometry being determined by the shape of the molecule is also observed on other weakly interacting metal-graphene systems *e.g.*, square lattice of FePc

on G/Pt(111) [61], F₁₆CuPc on G/SiC [87], CoPc on G/hBN [88] and hexagonal packing of C₆₀ on G/Cu(111) [89] and G/SiC [90,91]. Larger substrate corrugation can affect the lattice quality and domain size as demonstrated by CoPc self-assembly on G/SiO₂ and G/hBN. While CoPc forms a square lattice on both substrates, on G/SiO₂ the domain size is limited and there is disorder in the molecular ordering within the domains. On the geometrically smooth G/hBN substrate, the domain size is only limited by the size of the terraces of the underlying hBN [88].

On weakly interacting graphene stronger intermolecular interactions affect the self-assembly profoundly, *e.g.*, PTCDA on G/Pt(111) [92] and G/SiC [93–96], and PCTDI (perylene tetracarboxylic di-imide) on G/SiC [97] assemble in close-packed herringbone structures to maximize intermolecular hydrogen bonds (C–H ··· O and N–H ··· O, respectively). Additionally, the close-packed islands of PTCDA [94] and PCTDI [97] were observed to grow uninterrupted over step-edges and defects in the underlying graphene. These studies observed growth of multiple domains which were not aligned to the high-symmetry directions of graphene. These observations indicate that the molecular assembly on weakly coupled graphene is dictated by intermolecular interactions (vdW or hydrogen bonding) rather than molecule-substrate interactions.

In the case of graphene deposited on insulating substrates, the reduced screening can have an effect on the molecular self-assembly. This was demonstrated by Tsai *et al.*, who showed that F₄TCNQ on G/hBN forms close-packed islands at sufficiently high coverages [72] (Fig. 2h,i). The molecules pack in a head-to-tail fashion in compact islands, in contrast to F₄TCNQ on epitaxial G/Ru(0001) or G/Ir(111), where intermolecular repulsion dominates and neighboring molecules adopt a staggered geometry [85,98].

Interestingly, close-packed assemblies at sub-monolayer coverage can be formed even on the surface of strongly corrugated graphene by post-deposition annealing. On the G/Ru surface, PTCDA has been observed to assemble into a herringbone arrangement with only some of the TOP sites remaining empty after heating the substrate [65]. Similarly, pentacene [64] and C₆₀ [70] assemble into close-packed structures on G/Ru under high temperature deposition and annealing after deposition, respectively. The higher temperature causes the molecules to be mobile, facilitating their assembly into a close-packed, ordered structures corresponding to a higher adsorption energy per unit area.

3.3 Assembly engineering

It is possible to tailor molecular self-assembly by controlling the molecule-substrate interactions even on the strongly corrugated G/Ru surface. Yang *et al.* [61] demonstrated that for comparable coverage, a stronger (FePc), intermediate (MnPc), and weaker (NiPc and H₂Pc) molecule-substrate interactions lead to selective adsorption at FCC sites only, molecular chains in the valley regions, and a Kagome lattice, respectively. The molecule-substrate interaction can further be changed through metal intercalation under the otherwise weakly interacting G/Ir(111). The intercalation of Co and Fe leads to an enhancement of the moiré corrugation (to ~120-150 pm) and chemical binding between graphene and the substrate resulting in increased molecule-substrate interactions [99,100]. Bazarnik *et al.* [101] demonstrated that for low temperature deposition and at low coverages both CoPc and CuPc form one dimensional molecular chains in the lower lying region of the moiré formed on Fe (or Co) intercalated G/Ir. At a slightly higher coverage, the molecules begin to form hexagonal rings around the TOP region as shown in Fig. 4a. For room temperature deposition at a higher coverage, the molecules assemble into slightly distorted honeycomb lattices with empty TOP sites. Interestingly, when the periodicity of the moiré increases due to intercalation of a different rotational domain of

graphene on Ir(111), the assembled structure changes too. For intercalated graphene with a periodicity of 2.85 nm, the honeycomb lattice transforms into a Kagome lattice. An STM image of this assembly is shown in Fig. 4b.

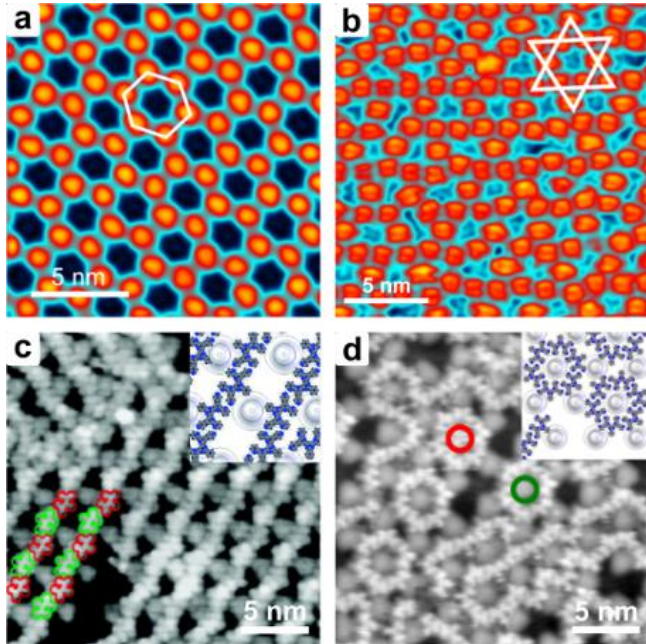


Figure 4: **Assembly engineering.** (a) CoPc molecules form a honeycomb lattice on G/Ir(111) intercalated with Co. Here the moiré periodicity is same as that of pristine G/Ir. (b) On G/Co/Ir(111) surface with larger moiré periodicity (2.85 nm compare to ~ 2.5 nm), the structure changes to a Kagome lattice [101]. (c) 2,4'-BTP molecules form long parallel chains along the symmetry direction of G/Ru [102]. (d) 3,3'-BTP molecules form rings and short chains on the surface [65]. The difference comes from the different position of the N atoms on the isostructural molecules which modifies the directional H-bonding. Adapted with permission from [65, 101, 102].

Further, self-assembled structures can also be modified by tuning intermolecular interactions on a given surface. For assemblies stabilized by directional H-bonds between the molecules, tuning the location of the electronegative species in the molecule can lead to completely different assembly. An example of this behaviour is the assembly of 2,4'-bis(terpyridine) (2,4'-BTP) [102] and 3,3'-bis(terpyridine) (3,3'-BTP) [65] on G/Ru. The molecule 2,4'-BTP assembles exclusively into linear, parallel chains lying along the symmetry axis of graphene (Fig. 4c); on the other hand, 3,3'-BTP forms rings and short chains centered around the TOP site (Fig. 4d). In both cases, adjacent molecules are seen to lie in an anti-parallel fashion, indicating the formation of C-H \cdots N hydrogen bonds. Such disparity in the assembly is simply due to the difference in the position of the nitrogen atoms in these two molecules.

3.4 Molecular templates

The templating effect of graphene and hBN is not confined to a monolayer of molecules. 2nd layer of C₆₀ molecules deposited on G/Ru surface shows highly-ordered assembly following the corrugation of the moiré pattern shown in Fig. 5a-b. However, the 3rd layer is no longer corrugated and reaches the bulk structure of C₆₀ as shown in Fig. 5c [69]. As another example,

the molecules of the second layer of CoPc on hBN/Ir(111) align themselves with the pores of the underlying moiré pattern [76].

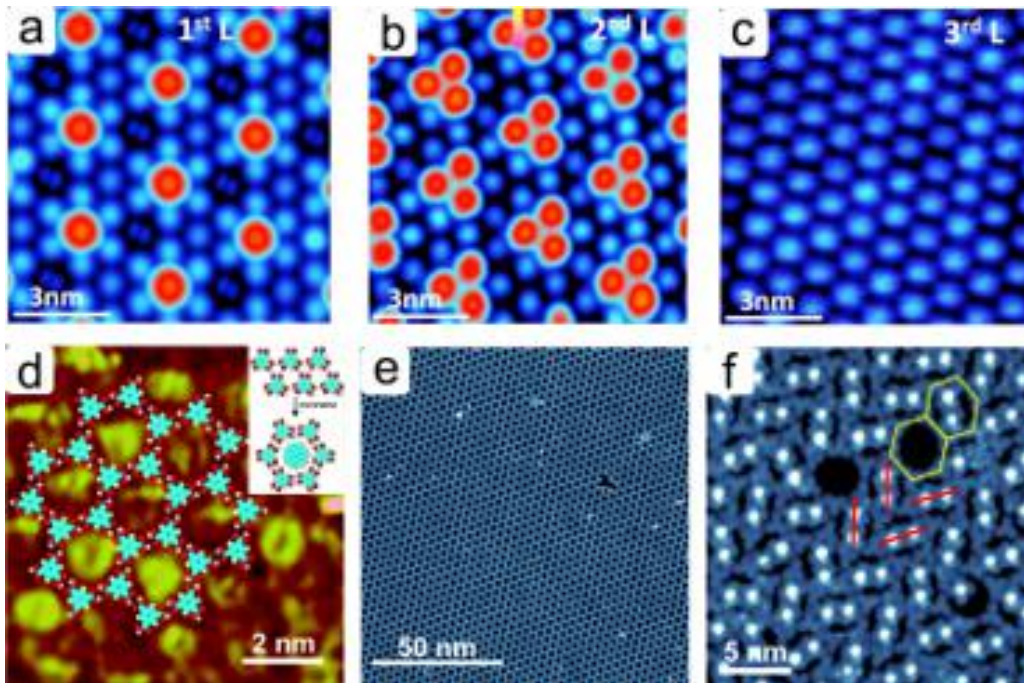


Figure 5: **Multi-layer templated assembly.** (a) C_{60} molecular assembly on G/Ru showing contrast in accordance with the moiré pattern; the molecule lying on TOP region of the moiré is the brightest. (b) The contrast is still visible in the second layer; however, three C_{60} molecules find places at hollow sites next to the brightest C_{60} of first monolayer and appear bright. (c) On the third layer the influence of moiré is insignificant [69]. (d) An otherwise close-packed assembly of trimesic acid (TMA) molecules on graphene on SiO_2 transforms into hexagonal structure on introduction of coronene molecules which occupy the pore of the assembly [103]. (e) Assembly of 1,3,5-benzenetribenzoic acid (BTB) molecules on G/Ir(111) showing long-range ordered network of hexagonal pores stabilized by H-bonding. (f) The flexible network hosts two CoPc molecules in each pore and CoPc assemblies in a herringbone pattern; the red lines highlight the arms of the herringbone [104]. Adapted with permission from [69, 103, 104].

Multi-layer growth on weakly coupled graphene is dependent on the assembling motif of the first adlayer. As mentioned in Sec. 3.1, PTCDA on G/SiC assembles in a herringbone pattern. The molecules in 2nd and 3rd layer mimic the herringbone arrangement of the first layer [93]. For pentacene, on the other hand, although the first layer of molecules lie flat with their long-axis aligned along the graphene zigzag direction, the second layer prefers to stand upright in a herringbone fashion [105] similar to on HOPG [106].

Molecular assembly with porous networks have often been used as a template to steer the assembly of other molecular species [2, 3]. Similar assemblies have been replicated on weakly coupled graphene to obtain nano-porous networks and use them in the so-called “host-guest” architectures. For example, sequential deposition of PTCDI and the 3-fold symmetric molecule melamine has been used to form hexagonal network stabilized by intermolecular hydrogen bonds on G/SiC [107]. Hexagonal porous network stabilized by hydrogen bonds have also been realized by 3-fold symmetric tricarboxylic acids *e.g.*, trimesic acid (TMA) and benzene-tribenzoic acid (BTB), which have been studied in detail on graphite and noble metal surfaces [108]. In a comparative study of TMA assembly at the liquid-solid interface on G/SiC and graphite, the

molecules were observed to assemble into a hexagonal network with a periodicity of ~ 1.6 nm and identical epitaxy on both surfaces [109]. In another study carried out at the solid-liquid interface on exfoliated graphene on silicon dioxide [103], deposition of TMA resulted in a close-packed structure. On subsequent deposition of coronene, the assembly changes to a honeycomb arrangement of TMA (periodicity ≈ 1.7 nm) with the coronene occupying the pores, as shown in Fig. 5d. This is an interesting example of the incorporation of the guest molecule causing a phase-change of the host network.

After deposition in UHV, 1,3,5-benzenetribenzoic acid (BTB) assembles into an extended hexagonal mesh with a periodicity of ~ 3.2 nm on G/Ir [104]. The network is quite stable and robust (Fig. 5e) with an estimated bonding energy of 1.95 eV per molecule, extending for hundreds of nanometers over step-edges of the underlying substrate. The periodic pores of the nanomesh can be used to pattern molecular assembly as demonstrated with CoPc. Remarkably two CoPcs could be hosted in a single pore without destroying the network - the strong yet flexible hydrogen bonds holding the network together undergo stretching to accommodate the guest molecules. When all pores of the BTB network are uniformly occupied with two CoPcs, the guest molecules are seen to arrange in a herringbone pattern as shown in Fig. 5f. The formation of the herringbone pattern is driven by the reduction of the energy cost associated with stretching and twisting the hydrogen bonds between the BTB molecules.

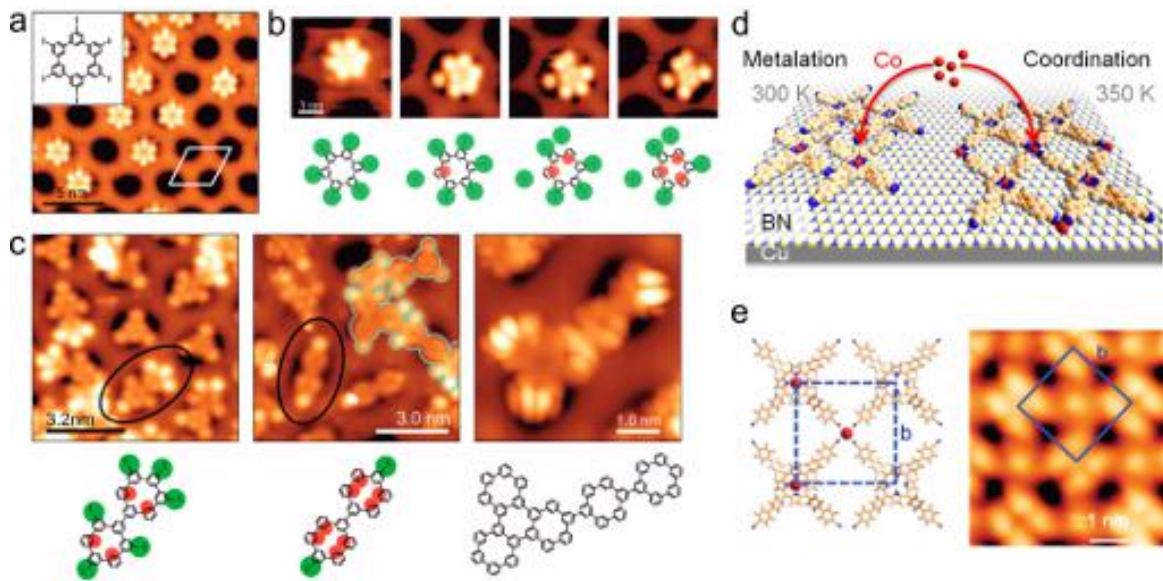


Figure 6: **Covalent reactions on 2D materials.** (a) I_6 CHP adsorption on hBN on Rh(111). (b) Step-by-step dehalogenation of a single I_6 CHP induced by voltage pulses from the STM tip. (c) Dehalogenation and subsequent cross-linking following thermal annealing to 550 K (left), 800 K (middle) and 850 K (right) [79]. (d) Schematic showing two ways of metal complexation of 2H-TPCN. At room temperature the Co atoms go to the tetrapyrrole pocket whereas on annealing to 350K they coordinate to the $-CN$ peripheral groups yielding a metal-organic coordination network. (e) Structure (left) and small-scale STM image (right) of the metallo-supramolecular network [81]. Adapted with permission from [79,81].

3.5 Covalently bonded structures

Several different coupling mechanisms for obtaining covalently bonded molecular assemblies have been demonstrated on metal single crystal substrates, where the catalytic activity of

the metal substrate is important. One of the better studied mechanisms is Ullmann-type coupling, where first a halogen - carbon bond in a precursor is cleaved, and the resulting radicals react to form carbon-carbon bonds [110–113]. This has been used to carry out on-surface polymerization [112,114], and in particular, synthesize atomically well-defined graphene nanoribbons of different widths and edge terminations [113,115–120].

The difficulties in using the radical coupling on surfaces other than bulk metals are highlighted by Dienel *et al.* [79]. They describe the reactivity of 5,5',5'',5''',5''',5''''-hexaiodocyclohexam-phenylene (I_6 CHP) on hBN/Ru (Figure 6a-c). I_6 CHP is typically very reactive on metal surfaces and dissociates all its iodine atoms on Cu(111), Ag(111), and even Au(111) already at room temperature [121]. The situation is different on hBN-covered metal surface as shown in Figure 6a, where it can be seen that following deposition at room-temperature, I_6 CHP remains undissociated. The reactivity of the I_6 CHP was tested using voltage pulses from the tip of the STM as shown in Fig. 6b. These experiments showed that the iodine atoms dissociate at alternating positions around the molecule and not more than three iodine atoms can be removed. The formed radicals are immediately stabilized by a bond formation of the radical site with the underlying boron atom [122]. This locks the molecule in position and consequently favours the remaining alternating sites for dehalogenation.

Dehalogenation can also be induced by thermal annealing [79]. Mild annealing (up to 550 K for 20 min) again results at most three iodines being cleaved (Fig. 6c (left panel)). After annealing to even higher temperatures (800 K and 850 K for 30 minutes, middle and right panels of Fig. 6c), more iodine atoms can be removed. Only at annealing temperatures of 850 K was it possible to produce iodine-free oligomers. However, the resulting structures do not yield the long-range order that can be observed on metal substrates after similar annealing [121]. On metal surfaces, the radicals are stabilized by bonding with the substrate, while the precursor molecules can still retain sufficient mobility to yield high quality structures.

Dehalogenation with brominated precursor molecule 1,3,5-tris(4-bromophenyl)-benzene (TBB) on hBN and graphene on Ni(111) has also been attempted [123]. Annealing the sample to 520-570 K results in debromination of the precursor molecules, which subsequently form covalently bound assemblies. However, these lack long range order observed with the same precursor molecules on coinage metals. Similar to I_6 CHP, limited mobility of the dehalogenated molecules due to a strong interaction with the hBN and graphene surfaces is likely to be responsible for the lack of long-range order. The strong interaction was further substantiated by DFT calculations showing a strong interaction between the phenyl unit and G/Ni(111) [123]. Finally, the authors argue that the order and spatial extension of the cross-linked molecules can be improved by a suitable choice of supporting metal surface for graphene and hBN, which would be more weakly interacting than Ni(111).

In contrast to the covalently bonded assemblies, metal coordination bonds have been demonstrated to yield molecular assemblies with long-range order on non-reactive hBN [81]. Urgel and co-workers investigated carbonitrile-functionalized porphyrin derivatives (2H-TPCN) cross-linked with Co atoms on epitaxial hBN on Cu(111) (Fig. 6d-e). Here, the molecule self-assembles into a densely-packed layer with a square unit cell. After evaporation of cobalt atoms onto the substrate at room temperature, metalation of the porphyrins is observed *i.e.*, Co-TPCN is formed. Coordination networks can be formed once submonolayer coverages of TPCN is exposed to Co atoms at 350 K [81]. Two different packing schemes are formed at this temperature: a densely-packed array representing the pure molecular phase and a network structure exhibiting a larger square unit cell and a central protrusion (blue square in Fig. 6e); the latter structure was assigned to a Co-directed assembly of a metalorganic coordination network. Surprisingly, they have 4-fold coordination in contrast to what is observed on metal

substrates.

Single-molecule reactions have also been investigated, for example, dehydrogenation of free-base phthalocyanine (H_2Pc) on epitaxial graphene [124]. In this particular case, graphene was used as an inert substrate that does not participate in the removal of the inner core hydrogens. Importantly, the formed radical did not bond with the underlying graphene, which allowed the study of the molecule in the same adsorption geometry before and after dehydrogenation. Another single molecule reaction was demonstrated by a novel cycloaddition scheme between various phthalocyanines and epitaxial graphene on Ir(111) [125]. This reaction could be driven reversibly by voltage pulses from the tip of a low-temperature STM. The reaction only occurs on a certain part of the graphene moiré pattern on Ir(111), which suggests that the bonding of the graphene with the underlying Ir(111) results in dangling bonds on the graphene surface.

4 Tunneling spectroscopy on 2D materials

Molecules physisorbed on a surface through van der Waals interactions retain their gas-phase electronic properties. This is no longer the case for molecules adsorbing through strong chemical bonds (*e.g.* covalent, metallic, and ionic bonds) [126]. An extensive review on molecule-metal bonds has been provided by Nilsson *et al.* [127]. Molecular orbitals of molecules adsorbed on metal surfaces are strongly hybridized (resulting in broadening, shifting, and mixing of the orbitals) because of the interaction with the continuum of electronic states in the metal [126, 128]. Typically, the spectroscopic signatures of the molecular orbitals are too broad to be reliably detected [128]. Molecules can be electronically decoupled from the metal substrate by the use of ultrathin insulating films that allow combining insulating surfaces and STM. The insulating layer (\sim few Å) can still be sufficiently thin to allow STM operation without difficulties. Ultrathin layers of conventional insulating materials, for example, alkali-halides [129–131], metal-oxides [73, 132–134], metal-nitrides [135, 136], passivated semiconductors [137, 138] have been used to study the properties of single atoms and molecules, and various aspects of molecular electronics in general.

The decoupling makes it possible to study molecules whose properties closely match those found in the gas phase (*e.g.* magnetic moment [139], fluorescence [132]). In a seminal experiment, Repp *et al.* [129] demonstrated that a NaCl bilayer is sufficient to electronically decouple pentacene molecules from the underlying Cu(111) surface. STS on the molecule shows sharp resonances in the differential conductance (dI/dV) spectra corresponding to temporary electron addition (positive sample bias) and electron removal (negative sample bias) to/from the molecule. These peaks are also termed positive (PIR) and negative ion resonances (NIR) referring to the transient occupation of the molecular orbitals [129, 140]. The first PIR at negative and the first NIR peak at positive bias correspond to the electron tunneling through the highest occupied molecular orbital (HOMO) and the lowest unoccupied molecular orbital (LUMO) of the molecule, respectively. While these peaks are often referred to HOMO and LUMO, energy difference between the PIR and NIR is not equal to the HOMO-LUMO gap. This so-called transport gap is larger than the HOMO-LUMO gap due to the Coulomb charging energies associated with adding/removing electrons to/from the molecule [141, 142]. It is more correct to think of the PIR and NIR as corresponding to the ionization potential and the electron affinity of the molecule, respectively (see [143–146] for details).

The very exciting aspect of STM is that it allows - in addition to measuring the energy positions of the molecular resonances - mapping out the molecular orbitals in real space. STM topographic images at bias values of PIR and NIR on a molecule deposited on a decoupling

layer resemble the HOMO and the LUMO orbitals of gas phase molecule as shown by Repp *et al.* [129]. These orbitals can be imaged with very high spatial resolution, especially using molecular modified tips [129, 131, 147].

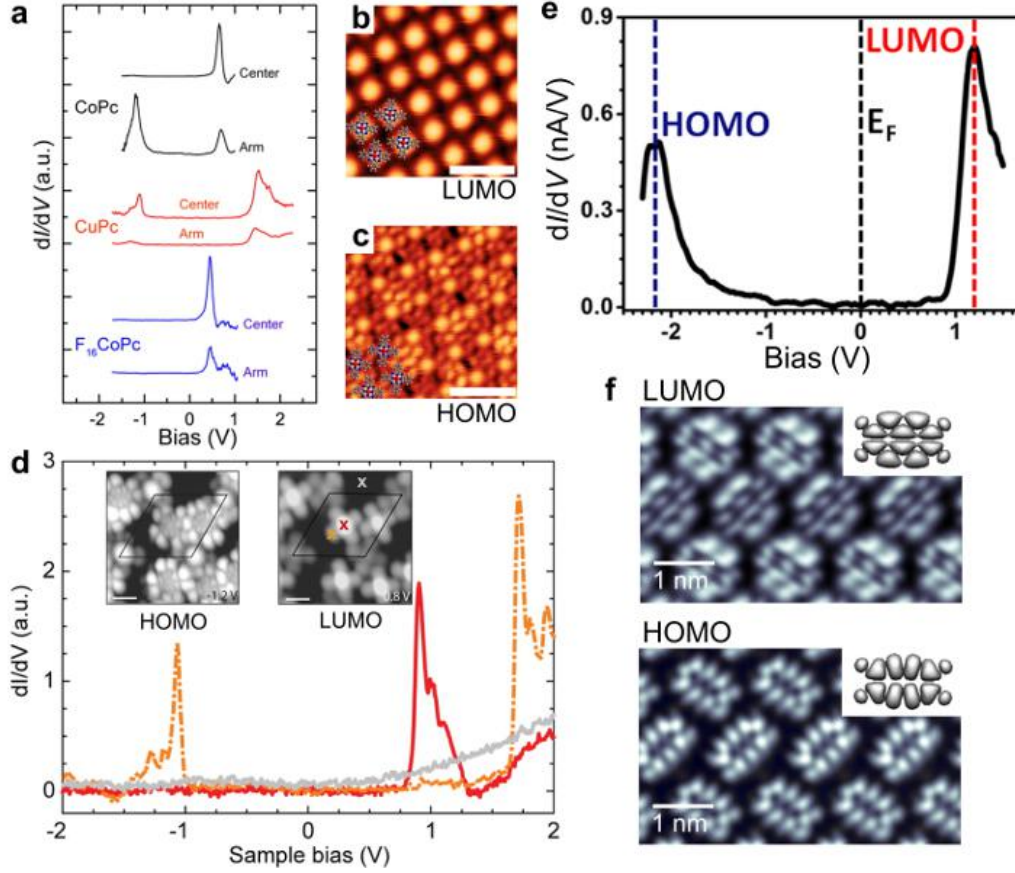


Figure 7: **Molecular orbital imaging.** (a) dI/dV spectra of CoPc, CuPc, and F_{16} CoPc molecules on G/Ir(111) recorded at the center and arm of the molecules. Peaks at positive and negative bias correspond to tunneling into the LUMO and HOMO, respectively. (b,c) STM images of CoPc assembly recorded showing the LUMO (b) and the HOMO (c). Scale bars are 3 nm [71]. (d) STS recorded on a CoPc molecule adsorbed on the wire site of hBN/Ir(111) moiré. Insets show STM images at -1.2 V and 0.8 V resembling HOMO and LUMO orbitals, respectively. Peak at 1.9 V corresponds to tunneling into LUMO+1 orbital [76]. (e) dI/dV spectrum of PTCDA molecules on G/Pt(111) showing HOMO and LUMO resonances. (f) STM images recorded at 1.34 V and -2.3 V show the LUMO and HOMO, respectively. Calculated orbitals are shown in the insets [92]. Adapted with permission from [71, 76, 92].

4.1 Orbital decoupling and orbital imaging on 2D materials

Similar to the above mentioned insulating layers, epitaxial graphene and hBN are also able to efficiently decouple the molecules from the underlying metal substrates by virtue of their chemical inertness and low density of states around the Fermi level. They can be used as a supporting surface to study the properties of single atoms and molecules for various aspects of molecular electronics. Experiments on C_{60} [89, 90], TCNQ [67], MPcs [71, 148], and PTCDA [66, 92, 93] adsorbed on epitaxial graphene indicate that molecules do indeed retain their intrinsic properties. Järvinen *et al.* [71] have carried out STS and orbital imaging of CuPc, CoPc and F_{16} CoPc

molecules deposited on G/Ir(111). The dI/dV spectra displaying the HOMO and LUMO resonances are shown in Fig. 7a. The value of the transport gap (HOMO-LUMO gap measured on G/Ir) should be smaller than in thick molecular films due to the additional screening from the graphene and the underlying metal substrate. As mentioned above, imaging at the bias voltages corresponding to the molecular resonances can be used to study the molecular orbital structure of each of the molecules. Fig. 7b-c shows HOMO and LUMO images of CoPc which closely resemble the DFT calculated orbitals for the gas-phase molecule. The HOMO orbital is delocalized over the π system of the carbon backbone while the LUMO orbital is localized on the central Co atom.

Similarly, Martínez-Galera *et al.* [92] demonstrated that graphene decouples PTCDA molecules from Pt(111) surface, as shown in Fig. 7e-f. Here too, HOMO and LUMO orbital images closely resemble the respective calculated orbital images for an isolated molecule. Zheng *et al.* [149] observed that the transport gap of PTCDA molecule increases from Au(111) (3.1 eV) to HOPG (3.5 eV) to semi-conducting WSe₂ (3.7 eV) surface. These observations were substantiated using DFT calculations that take image charges at the substrate into account; this highlights the importance of substrate-induced screening in STM studies of single molecules. Cho *et al.* [90] studied C₆₀ molecules deposited on G/SiC surface, which show three peaks at -2.7 V, 0.8 V, and 1.6 V. These features are likely to correspond to HOMO, LUMO, and LUMO+1; again, the HOMO-LUMO gap of 3.5 eV is higher than on Au(111) surface (2.7 eV [150]). A number of UHV-based non-STM studies have also been carried out to discuss the decoupling of molecules due to epitaxial graphene layer [148, 151–153].

As discussed above, molecules adsorbed on epitaxial graphene are weakly coupled with the substrate and retain their intrinsic properties. The same is true for graphene deposited on an insulator *e.g.*, SiO₂ or hBN. CoPc molecules deposited on these substrates show life-time limited lorentzian lineshapes [88]. Graphene on insulating substrate makes it possible to tune the charge carrier concentration through external doping. Voltage on the back gate shifts the graphene Fermi level w.r.t. the Dirac point and hence, the molecular resonances also shift. Riss *et al.* demonstrated STM measurements with a gate electrode by performing experiments on 1,3,5-tris-(2,2-dicyanovinyl)benzene (CVB) molecules on a G/hBN substrate [154]. They showed that the molecular resonances could be shifted by ca. 200 mV by sweeping the gate voltage from 0 V to 60 V. This suggests controlling charging in single molecules and molecular assemblies while simultaneously resolving their LDOS with sub-molecular spatial resolution.

In two separate reports, Schulz *et al.* [76] and Joshi *et al.* [77] have shown that CoPc molecules deposited on hBN/Ir surface and 2H-P molecules deposited on hBN/Cu surface are also decoupled from the metal surfaces due to the epitaxial hBN layer. Fig. 7d shows HOMO (-1.1 V) and LUMO (0.8 V) peaks in the STS spectra recorded on CoPc molecules adsorbed on the wire region of the hBN moiré and the STM images recorded at the corresponding bias voltages. These sharp resonances have life-time limited lorentzian shape and enable high energy resolution spectroscopy of isolated molecules [76, 155]. Similarly, sharp HOMO and LUMO peaks were observed for the 2H-P molecules on the hBN/Cu surface [77]. Finally, the presence of work function modulation over the moiré of hBN on metal surface leads to site-selective charging of the molecules which will be discussed in the next section.

4.2 Site-selective gating and charging

We have discussed site-selective adsorption of molecules on 2D materials which is related to periodic modulation of electronic and chemical properties across the moiré pattern. This also results in a modulation of molecular orbitals of the molecules and in some cases, to site-selective

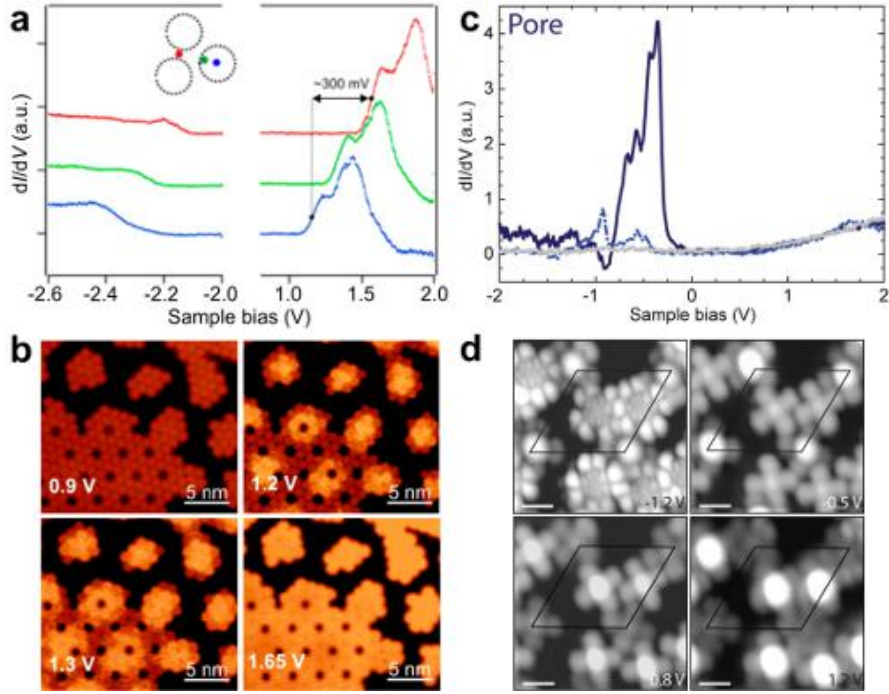


Figure 8: Site-selective modulation of molecular orbitals. (a) dI/dV spectra recorded on porphine molecules located at pore (blue), rim (green), and bridge (red) sites of the hBN moiré. Across the moiré, the energy of LUMO varies by about 300 mV and the HOMO-LUMO gap increases from pore to the bridge site. (b) Bias dependent imaging shows that the molecules at the pore region are brighter at 1.2 V and the brightness extends away as the bias is increased. At 1.65 V all the molecules have similar brightness [77]. (c) dI/dV spectrum recorded at the center of CoPc molecules on the pore site of the hBN/Ir(111) moiré shows peak at -0.4 V. For dI/dV spectra on molecules on wire site see Fig. 7d. The molecule on the pores are negatively charged and LUMO (of the neutral CoPc on wire site) has shifted below Fermi level. (d) Bias dependent STM imaging show different orbitals participating at different biases. Black rhombus shows the unit cell of hBN/Ir(111) moiré. While the molecules at the pore resemble LUMO, at the wire site they resemble HOMO at -1.2 V. As the bias is increased to 0.8 V and further to 1.2 V, the molecules at the wire site resemble LUMO and the molecules at the pore site resemble higher order orbitals [76]. Adapted with permission from [76,77].

charging of molecules. Already on a weakly interacting system, G/Ir(111), Järvinen *et al.* [71] observed that the LUMO resonance peak of CoPc and F_{16} CoPc is modulated by as much as 200 mV across the moiré. The molecules adsorbed on the TOP region of the moiré showed the LUMO peak at higher energy in line with the fact that the TOP region has a larger work function. However, the HOMO did not shift as much, i.e. the HOMO-LUMO gap is increased on the TOP region. Thus the rigid shift due to work function difference (estimated 60 meV across the moiré) alone is not sufficient to explain these orbital shifts. Other possible explanation are a change in the screening due to modulation of graphene - Ir distance across the moiré, modulation of bonding character of graphene across the moiré and spatially different symmetry of molecular resonances.

Compared to G/Ir, epitaxial hBN on different metals exhibits stronger work function modulation and geometric corrugation across moiré pattern, which would be expected to lead to more drastic effects on the orbital energies. A number of molecules deposited on different hBN surfaces [76,77,81,156] show such site-specific modulation of molecular orbitals. Therefore, many

interesting physical effects become visible. Joshi *et al.* [77] report modulation of the position of the molecular orbitals and the HOMO-LUMO gap across the moiré of hBN/Cu(111). Fig. 8a shows dI/dV spectra recorded on 2H-P molecules adsorbed on different sites of the moiré. The LUMO peak is shifted up by as much as 300 mV for the molecules lying on the bridge compared to the pore site. This shift is smaller for the molecules lying on the rim of the moiré. The shift of the LUMO matches the work function difference between the pore and the bridge site (~ 300 meV), indicating that the change in the orbital energy simply reflects the local vacuum level alignment. However, the HOMO-LUMO gap was also found to be modulated with respect to the moiré as shown in Fig. 8a. The smallest gap is observed for the molecules on the pore region. Here too, charge screening has to be taken into account to explain the shifts. The energy shift of the LUMO orbital is also observed in the bias dependent STM imaging as shown in Fig. 8b. The molecules on the pore region have lowest lying LUMO and appear bright first in STM images. LUMO orbitals of other molecules get inside the bias window as the sample bias is increased and subsequently at 1.65 V, the whole monolayer has similar brightness. These results are not particular to 2H-P; 2H-TPCN and Co-TPCN molecules [81] adsorbed on hBN/Cu(111) show similar modulation of LUMO peak and HOMO-LUMO gap.

The effect of work function modulation across moiré is even stronger for CoPc molecules adsorbed on hBN/Ir(111) surface. Schulz *et al.* [76] performed STS on CoPc molecules adsorbed on the pore and on wire site of the moiré. While the molecules on the wire site (see Fig. 7d) show peaks at -1.1 V (HOMO), 0.8 V (LUMO) and 1.7 V (LUMO+1), the molecules on pore site shows a strong peak at -0.4 V as shown in Fig. 8c. Bias dependent STM imaging show different orbitals participating at different biases as shown in Fig. 8d. While the molecules at the pore resemble LUMO, at the wire site they resemble HOMO at -1.2 V. As the bias is increased to 0.8 V and further to 1.2 V, the molecules at the wire site resemble LUMO and the molecules at the pore site resemble higher order orbitals. As the orbital mapping at -0.4 V resembles the LUMO of the wire site (neutral CoPc) molecule, the peak is attributed to the LUMO shifted below the Fermi level due to electron transfer from the substrate to the molecule. Work function of pore site is smaller by 0.5 eV from the wire regions - this is sufficient to induce charging. The spectra recorded on the lobes of the charged molecule display additional resonances that cannot be explained within the simple single-particle picture [155]. Instead, the results can be understood as a series of many-body excitations of the different charge states of the molecule. These results rely on the possibility of carrying out high-resolution STS and the fact that different charge states of the same molecule can be probed in chemically equivalent environment, which are made possible by the hBN insulating film.

The decoupling by hBN results in sufficiently narrow widths of the molecular resonances and vibronic features in the spectra are easily resolved. The vibronic features result from elastic tunneling through one of the molecular resonances while simultaneously exciting a molecular vibration [157, 158], which manifests as satellite peaks around that molecular resonance peak with a spacing determined by the energy of vibrational mode that is excited [159–161]. The vibronic progressions of LUMO orbitals of CoPC molecules on the wire and pore sites of the moiré formed by hBN/Ir are evident in Fig. 7d and Fig. 8c [76].

4.3 Tip-gated charging

Molecules adsorbed on thin insulating layers probed by STM constitute a double-barrier tunnel junction, where a part of the voltage applied between the STM tip and the substrate drops between the molecule and the substrate. This can give rise to charging, when a molecular orbital close to the Fermi level of the substrate crosses the Fermi level due to finite voltage

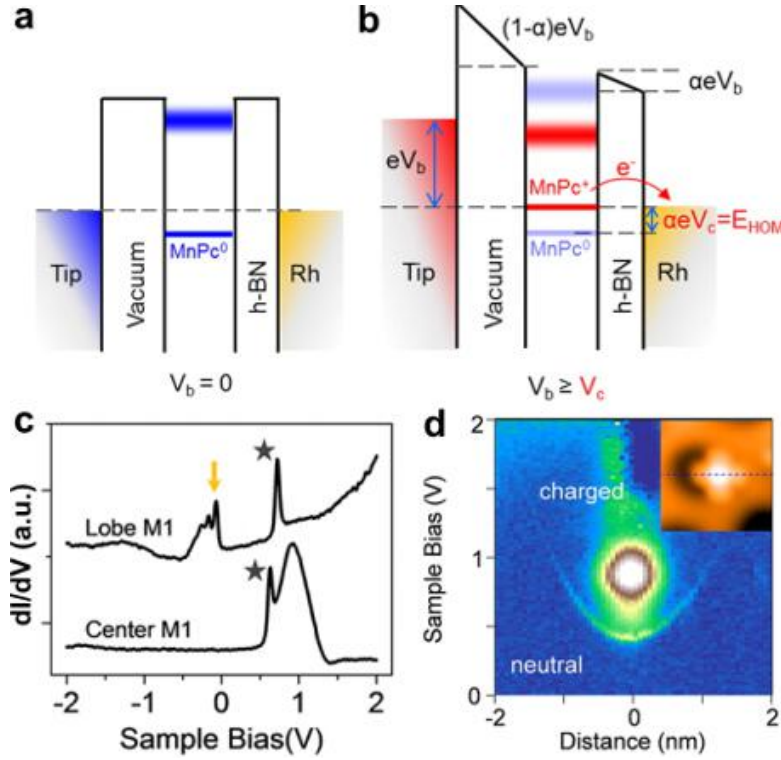


Figure 9: **Tip-gated charging.** (a) Energy level diagram for neutral MnPc in STM junction depicting the formation of double-barrier tunnel junction. The HOMO (shown in blue) of the molecule is very close the Fermi level. (b) Energy level diagram corresponding to tip-gated charging of the MnPc molecule at positive sample bias, V_b . Here, the HOMO crosses the Fermi level (shown in red) and the molecule loses an electron to form MnPc^+ . α is the lever-arm factor. (c) dI/dV spectrum recorded on the lobe shows HOMO close to Fermi level (indicated by yellow arrow) and a sharp peak at positive bias (indicated by asterisk) corresponding to the tip-gated charging. Spectrum at the center of the molecule shows broad LUMO peak along with the charging peak. (d) Stacked dI/dV spectra taken across the molecule shows the locus of the charging peak and LUMO orbital. Adapted with permission from [156].

drop across the insulating layer [162] (schematic in Fig. 9a-b). The charging results in a modification of the potential barrier profile of the junction [163] and subsequently results in a sharp change in the dI/dV spectrum. Liu *et al.* shows this can be observed with MnPc molecules adsorbed on hBN/Rh(111) [156]. One of the adsorption sites across the moiré shows the molecules with a bright centre in a neutral state but having their HOMO level close (~ 100 meV) to the Fermi energy (shown by yellow arrow in Fig. 9c). This orbital is brought above the Fermi energy at positive bias and a sharp peak (indicated with asterisk) appears in dI/dV spectrum along with LUMO orbital of the molecule. The bias voltage corresponding to the charging peak depends on: (i) the exact location of the HOMO, (ii) the location of the STM tip, and (iii) the relative potential drop across the tip-molecule and molecule-substrate junctions (lever-arm factor). Figure 9d shows stacked dI/dV spectra recorded across the molecule with a topographic image shown in the inset. The locus of the charging peak (large dI/dV feature) seems to follow parabolic arc along the bright spot at the centre, which corresponds to the LUMO of the molecule. Above the parabola, the molecule is in the charged state and below it is neutral.

5 Band structure engineering and doping of graphene

The electronic properties of monolayer graphene are described by its conical band structure at the K and K' -points of the Brillouin zone. The linear dispersion of the charge carriers near the Dirac points gives graphene many of its fascinating electronic properties *e.g.*, high electron mobility and ambipolar transport [164]. However, application of graphene in practical electronic devices has still not been realized as it requires two things: precise control over the type and concentration of charge-carriers and opening a sizeable band gap in the graphene band-structure [165]. Furthermore, these goals should be achieved through methods that are inexpensive and scalable and do not compromise the wonderful electronic properties of graphene. Many schemes have been used to introduce a band-gap in graphene. Quantum confinement of charge carriers in lithographically defined graphene nanostructures and unzipped carbon nanotubes can be used to create a band gap [166–171], but these methods cannot be used to achieve atomically well-defined nanoribbon edges. Bottom-up on-surface synthesis offer unprecedented control over the GNR width and edge termination [113, 117, 119, 120]. However, contacting these very narrow ribbons is still a major technological challenge [172]. Recently, experiments on graphene on hBN devices have shown band gaps of up to 300 meV depending on the misalignment angle of the two lattices [173]. The exact mechanism of the gap opening is still under debate, with both breaking of the graphene sublattice symmetry due to the underlying hBN [173] and biaxial strain [174] have been proposed.

Covalent functionalization can also be used for both gap opening and doping and band gaps greater than an eV have been reached through partial rehybridization of the sp^2 carbon atoms to sp^3 *e.g.*, by hydrogen [17] or fluorine [175]. Substitutional doping with boron and nitrogen atoms to obtain hole (p-type) or electron (n-type) rich graphene has also been demonstrated [176–179]. However, these methods potentially disrupt the extended π -conjugation of graphene and lead to a degradation of graphene’s exceptional electronic properties. On the other hand, physisorbed molecules interacting with graphene through weak vdW interactions are expected to offer a route to modify graphene’s electronic properties without degrading its desirable properties, even under high charge carrier density.

Doping of graphene by physisorbed molecules can be achieved easily by means of interfacial charge transfer, which can be tuned through the energy level alignment of the molecular frontier orbitals with respect to graphene’s Fermi level (E_F , which is ≈ 4.5 eV for free-standing graphene [180]) as shown in Fig. 10a. If the electron affinity (EA) of the molecule is larger than graphene work function, the molecule will accept electrons from graphene and make it hole-doped (*i.e.*, p-doped). Conversely, if the ionization potential (IP) of the molecule is smaller than graphene work function, the molecule will donate electrons to graphene, making it electron-doped (*i.e.*, n-doped). The EA and IP of the molecule will be modified from their gas-phase values by screening due to the graphene surface. While DFT calculations including vdW corrections are the best available theoretical means to estimate the amount of charge transfer between a given molecule and free graphene surface [181–183], they can also be estimated based on photoelectron or Raman spectroscopy or by transport experiments. In addition to doping, periodic potential modulation has been proposed as means of breaking the sub-lattice symmetry in graphene [184]. An adlayer with the correct symmetry and period can potentially lead to a band-gap in graphene.

To date, many small gas molecules and hydrocarbons have been used to dope graphene with both donor- (*e.g.*, NH_3 [185], polyethyleneimine [186], naphthalenediamine, dimethylanthracene [187]) and acceptor-type dopants (*e.g.*, H_2O [188], O_2 [189], diazonium salts [186], pyrenetetrasulfonic acid, dibromoanthracene [187]). These have resulted in changes in the

charge carrier density without degradation of electron mobility. Moreover, this type of doping is reversible as the weakly absorbed molecules can desorb by gentle annealing. While there is an enormous body of literature on functionalization of graphene with molecules (see [22–26] for reviews), here we only concentrate on well-defined systems with molecules forming large-scale, periodic lattices on graphene.

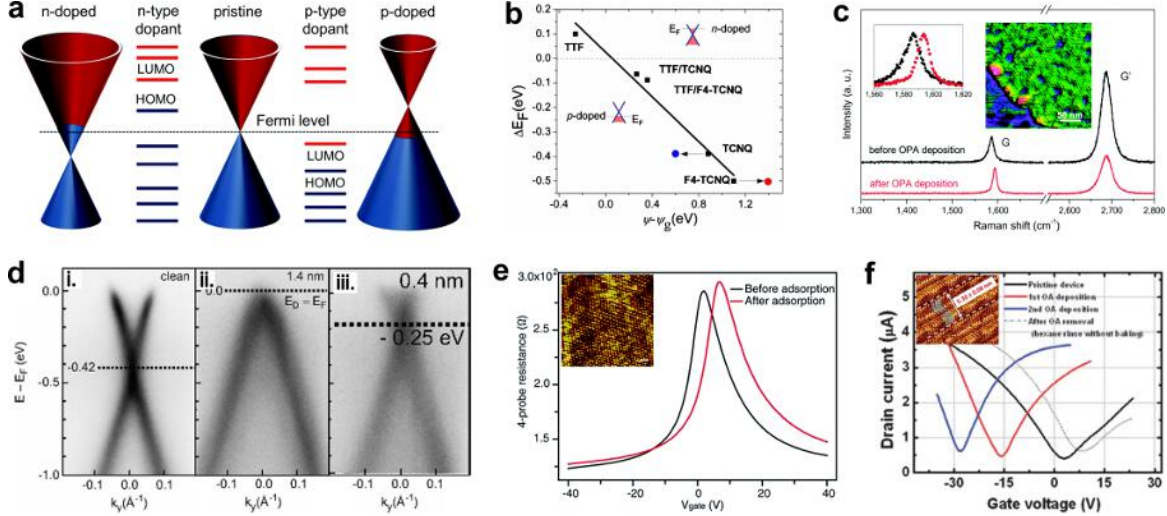


Figure 10: Charge donor and acceptors on graphene. (a) Schematic of doping of graphene by molecules: molecules with LUMO lying at energy lower than graphene Fermi level E_F spontaneously accept electrons from graphene making the latter p-doped (right side). Conversely, molecules with the HOMO above graphene E_F spontaneously donate electrons to graphene making the latter n-doped (left side) [21]. (b) Theoretical data points (black squares) on acceptors (TCNQ, F₄TCNQ), donors (TTF) and their salts on graphene. The abscissa gives change in E_F and, ordinate gives change in work-function of graphene after deposition of molecules [190]. (c) Raman measurements showing p-doping effect of OPA on graphene. Inset shows AFM image of OPA assembly on G/SiO₂ [191]. (d) ARPES data of (i) G/SiC ($E_F = -0.42$ eV) which is intrinsically n-doped, (ii) after deposition of 0.8 nm of F₄TCNQ on it (E_F saturates at 0 eV) and, (iii) after deposition of 0.4 nm of TCNQ on it (E_F saturates at -0.25 eV) [192]. (e) Electrical transport measurements on a G/SiO₂ FET before and after treatment with TMA indicating p-doping. Inset shows STM image of TMA assembly at solid-liquid interface on G/SiC. [103]. (f) $I_{SD} - V_G$ curves of G/SiO₂ FET before and after repeated cycles of treatment with OA indicating increased n-doping and improved mobility with each cycle. Inset shows STM image of OA assembly on HOPG [193]. Adapted with permission from [21, 103, 190–193]

Measuring doping level of graphene with tunneling spectroscopy is non-trivial in particular for graphene buried under a molecular adlayer with conflicting results in the literature for *e.g.*, PTCDA adsorption [94, 194]. Assessing the effect of molecular layers on the band structure of the underlying 2D material is perhaps better carried out using photoelectron spectroscopy (PES), in particular angle-resolved photoelectron spectroscopy (ARPES). Synchrotron based high-resolution PES shows that the work function of G/SiC shifts up by ~ 0.25 eV upon deposition of 1 ML of PCTDA, indicating very weak hole transfer from the molecule [93, 195]. The fact that the graphene band structure remains unaltered after deposition of PTCDA or pentacene [196] has been utilized in using them as seeding layer for atomic layer deposition (ALD) of thin dielectric layer (aluminum oxide) [96] or as a protecting layer for the graphene.

C₆₀ acts as a weak electron acceptor (EA ≈ 3.7 eV). High resolution PES data [197] on

G/SiC show a ~ 0.15 eV upshift of the work function of the system compared to clean epitaxial graphene; this indicates very weak p-doping of graphene. Raman spectroscopy and terahertz conductivity measurement on graphene on SiO₂ confirm a weak p-doping effect due to C₆₀ deposition (estimated as $\sim 0.04e$ transferred to each molecule) [198]. Additionally, the carrier mobility increases by ~ 1500 cm²/Vs - the authors hypothesize that it is due to screening of long-range scatterers (charged impurities at G/SiO₂ interface) by the molecules. Two other organic molecules - octadecylphosphonic acid (OPA) (Fig. 10c) [191] and trimesic acid (TMA) (Fig. 10e) [103] assemble into well-ordered structures and cause p-doping of graphene as shown by transport and Raman measurements. respectively.

We now turn our attention to organic molecules which are strong electron acceptors *e.g.*, tetracyanoquinodimethane (TCNQ), fluorinated tetracyanoquinodimethane (F₄TCNQ), and tetracyanoethylene (TCNE). Doping of graphene due to interfacial charge transfer by these molecules has been topic of many theoretical studies [199,200]. Sun *et al.* [190] performed DFT calculations showing that F₄TCNQ, which has a higher electron affinity than TCNQ [201], is expected to accept more charge (0.4e) than TCNQ (0.33e) (Fig. 10b). This prediction is confirmed by the ARPES experiments by Coletti *et al.* on G/SiC [192]. G/SiC is intrinsically n-doped with the Dirac point 0.42 eV below the E_F (Fig. 10d (i)). Deposition of F₄TCNQ drives the Dirac point towards E_F ; it saturates at E_F after deposition molecular layer with a nominal thickness of 0.8 nm (Fig. 10d (ii)). This indicates a neutralization of the graphene surface due to p-type doping from the molecule. For TCNQ however, the Dirac point saturates at 0.25 eV below E_F (Fig. 10d (iii)). Thus, the p-type doping from TCNQ is weaker than its fluorinated counterpart. XPS data of F₄TCNQ on G/SiC further reveals that the charge transfer takes place exclusively through one pair of the terminal cyano groups with the molecules adsorbing in an upright configuration at high coverage. Another synchrotron-based PES study indicates that the work function of G/SiC (4 eV) increases with increasing surface coverage of F₄TCNQ, saturating at 5.3 eV after deposition of a monolayer [197]. This is associated with a 0.5 eV shift of the graphene related C1s peak to lower binding energy. The authors concluded that this is due to charge accumulation at the G/SiC interface due to strong hole doping by the molecule.

Theoretical studies of the electron donating tetrathiafulvalene (TTF) molecule on graphene have predicted that it donates 0.1e to graphene, making the latter n-doped [190,200]. UHV based XPS data of chemically exfoliated graphene dispersed with TTF indicates the presence of both uncharged and positively charged sulphur [202]. This indicates electron donation to graphene by TTF.

Vanadyl phthalocyanine (VOPc), a member of the phthalocyanine family which assembles into close-packed geometry on graphene, is seen to dope it with electrons [203]. Kelvin probe force microscopy (KPFM) on exfoliated graphene on SiO₂ reveals that deposition of VOPc results in an increase of the contact potential difference (CPD), indicating transfer of electrons from the molecules to graphene. Mono- and bilayer graphene are more strongly electron-doped by the molecules compared to thicker graphene layers. $I - V$ measurements on graphene FETs show an downshift of the V_{CNP} by ~ 9 V, without any degradation of carrier mobility, confirming the n-doping. Based on the experimental data, the authors concluded that each molecule donates about 0.04e to graphene. N-doping of graphene has also been found with adsorption of oleylamine which assemble in lamellar nanostrips on G/SiC [193]. The V_{CNP} of G/SiO₂ FET shifts down by 19 V after deposition of the molecules from solution; this is associated with a two-fold increase in mobility.

The discussion so far has concerned molecular adlayers on graphene; now we turn to the effects of self-assembled monolayers (SAMs) under graphene. Silane-based molecules with a long alkyl chain capped with functional groups have been used to treat SiO₂ surface to tune

its properties. The silane group bonds covalently with the silicon dioxide surface neutralizing the Si- and O- dangling bonds and passivating the surface [204]. These dangling bonds facilitate p-type doping of graphene deposited on SiO₂ and act as long-range Coulomb scatterers reducing the electron mobility. Graphene should therefore be less p-doped and have better mobility, which was confirmed by Lee *et al.* [205]. Raman spectroscopy of graphene transferred onto untreated and SAM passivated surfaces suggests a decrease of surface induced p-doping. The results are confirmed from ultraviolet photoemission (UPS) data which show a concomitant decrease of the work-function of graphene to almost free-standing values. Finally, $I - V$ measurements on graphene FETs show devices with SAMs have V_{CNP} close to zero back-gate voltage and an increased electron mobility with a higher packing density of the SAM leading to better device performance (Fig. 11a).

SAMs offer the possibility to tune the reactivity of the surface by different functional groups. For example, SAMs with electron donating NH₂- groups n-dope graphene [206]. This was demonstrated by Raman and UPS measurements, where CVD-graphene transferred onto NH₂-SAM modified surface was n-doped compared to untreated or CH₃-SAM modified surface. $I - V$ data in Fig. 11b, shows that NH₂-SAM causes reduction of V_{CNP} to large negative voltages, confirming the n-doping effect. Based on a study of SAMs with several different functional groups, Yokota *et al.* [207] concluded that the doping effect can be related to the induced dipole moment in the SAM. For certain functional groups (NH₂C₆H₄- and C₈-SAM), the dipole points towards the graphene while for others (NH₂C₃H₆- and the fluorinated F₁₃-SAM), the direction of the dipole is opposite. It was found that the SAMs of first kind n-dope graphene, bringing the carrier-density to near pristine levels while the latter p-dope graphene. In another study of $I - V$ characteristics of CVD-graphene on SiO₂ passivated with different SAMs, the authors [208] concluded that for some SAMs (strongly p-doping CF₃-SAM and slightly n-doping CH₃-SAM), the doping is due to the dipole moment. But for SAMs with strong electron donating (strongly n-doping NH₂-SAM) or accepting groups (weakly p-doping H₃N⁺-SAM), the doping is due to interfacial charge transfer.

While opening a band-gap in monolayer graphene by self-assembled molecular layers has not yet been demonstrated, this has been achieved in the case of bilayer graphene (BLG). Band gap in BLG can be opened by breaking the equivalence of the individual layers by application of an external electric field perpendicular to the layers [11], which has been shown by external electrostatic gates [210]. However, this approach requires application of complex lithographic processes and high electric fields. An alternative way to achieve this would be to generate an interlayer charge asymmetry by individually tuning the polarity and concentration of charge carriers in the top and bottom graphene layers through chemical doping. Doping by F₄TCNQ has been seen to open a band-gap in epitaxial BLG on SiC [192] (Fig. 11c). BLG/SiC is intrinsically n-doped with a band-gap caused by electric dipoles at G/SiC interface which break the interlayer symmetry. This manifests in ARPES data as a gap of about 0.116 eV; the Dirac point lies mid-gap, about -0.3 eV below the E_{F} . Increasing F₄TCNQ coverage drives the Dirac point close to E_{F} (*i.e.*, a reduction in n-doping) with an increase in the band-gap. Finally at about 2 ML coverage, the effects saturates giving a final band-gap of 0.275 eV. The authors proposed that an additional dipole at the molecule-graphene interface increases the electrostatic asymmetry, resulting in an increase of the band-gap. Deposition of F₄TCNQ is also seen to open a band-gap in exfoliated BLG [209] (Fig. 11d) on NH₂-SAM functionalized SiO₂ substrate. As seen from $I - V$ measurements, SAM functionalization leads to n-doping of the graphene and compared to an unpassivated surface, the resistance at V_{CNP} is higher. Deposition of F₄TCNQ is seen to drive V_{CNP} to larger positive values with an accompanying increase of resistance at V_{CNP} . Based on a model calculation, the authors estimated the largest achieved gap as 0.124

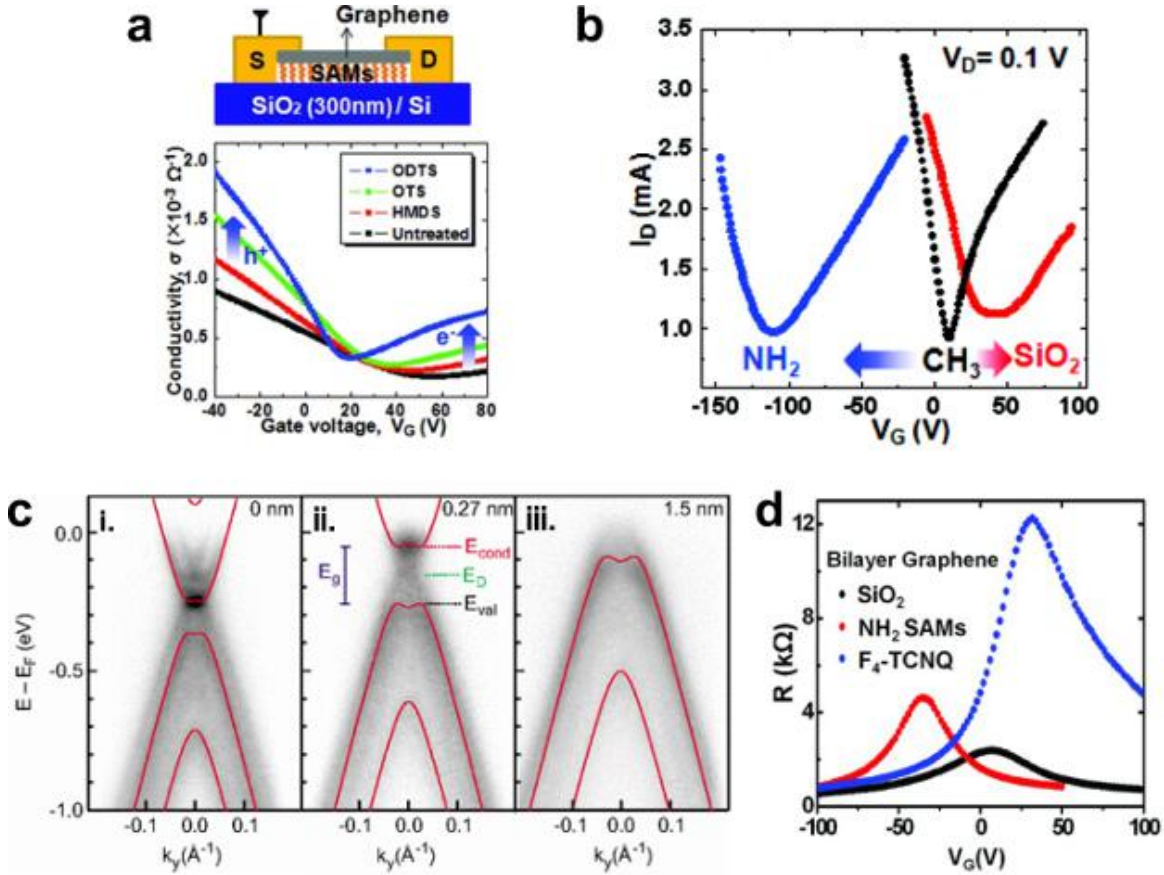


Figure 11: **Self-assembled monolayers and band gap opening in bilayer graphene.** (a) (top) Schematic of a graphene FET on SiO₂ treated with a SAM. (bottom) Transfer characteristics of graphene on untreated SiO₂ and graphene on SiO₂ treated with a SAM of increasing alkyl chain length (HMDS < OTS < ODTS) showing a concomitant decrease of V_{CNP} towards 0 V and increasing mobility [205]. (b) $I_{SD} - V_G$ curves of graphene on untreated SiO₂ (heavily p-doped), and on CH₃-SAM (almost neutral) and NH₂-SAM treated SiO₂ (heavily n-doped) [206]. (c) ARPES data of (i) BLG/SiC ($E_F = -0.3$ eV, $\Delta E_g = 116$ meV), (ii) after deposition of 0.27 nm of F₄TCNQ and, (iii) after deposition of 1.5 nm of molecule. ΔE_g saturates at 275 meV and E_F moves in-gap [192]. (d) Transfer characteristics of a BLG FET on SiO₂ treated with NH₂-SAM shows n-doping and two-fold increase in R_{CNP} (compared to BLG on native dioxide). Deposition of 10 Å of F₄TCNQ on it results in p-doping and about six-fold increase in R_{CNP} (compared to initial state) [209]. Adapted with permission from [192, 205, 206, 209].

eV. Accompanying infrared absorption data gave an estimate of the maximum optical band-gap of 0.210 eV. In both cases, the gap increased with increasing F₄TCNQ surface coverage. The authors concluded that that NH₂-SAM gives stable n-doping to the bottom graphene layer and F₄TCNQ deposition leads to p-type doping of the top layer: the increased asymmetry results in a concomitant increase in the gap.

6 Summary and outlook

Molecular self-assembly has been typically studied on metal surfaces or on graphite, where the focus has been on understanding the fundamentals and to investigate in detail the structure

of the assemblies. In the case of bulk substrates, molecular self-assembly cannot be used for a profound modification of the substrate electronic structure beyond doping or quenching surface states. Alternatively, molecular layers can be used as templates for patterning the deposition of subsequent layers.

Two-dimensional materials consist of only surface atoms, and hence, adsorption of a molecular layer can completely change their electronic response. This is a strong motivation to study molecular self-assembly on 2D materials. Understanding the formation of molecular assemblies, which can differ strongly from the corresponding systems on a metal substrate, is progressing especially in the case of epitaxial graphene and hexagonal boron nitride substrates. Close-packed molecular assemblies without intermolecular bonds or hydrogen-bonded networks are relatively well-understood. More strongly linked assemblies, in particular covalently bonded systems are still a virtual *terra incognita* and we lack even basic understanding of chemical reactions where the substrate is involved.

Compared to the close-packed metal surfaces, 2D materials present an inert surface on which the electronic properties arising from the self-assembled molecules are preserved. Beyond its obvious importance in fundamental research on the electronic properties of molecular materials, this presents an unique opportunity to test monolayer thick, all-organic electronic devices. These could also be incorporated into van der Waals heterostructures (*i.e.*, stacked layers of 2D materials), for additional stability and functionality. The immense flexibility in choosing the constituents of such hybrid materials makes a strong case for further studies in this field.

Molecular adlayers can help enable novel applications that are only made possible through the unique properties of 2D materials. For example, molecular layers can enable strong and precise doping profiles, which are important in formation of sharp p-n-junctions. Further-reaching potential applications include profound modifications of the band structure of 2D materials by, *e.g.* imposing a periodic potential modulation through molecular self-assembly to generating totally novel materials where the properties of the 2D substrate and the molecular layer strongly hybridize. Beyond the application of functionalized 2D materials in the fields of catalysis, sensors, and flexible and transparent electronic materials, the combination of molecular adlayers and 2D materials in hybrid heterojunctions can open a hitherto unknown vista of materials with exciting electronic properties.

7 Acknowledgements

This research was supported by the European Research Council (ERC-2011-StG No. 278698 PRECISE-NANO), the Academy of Finland (Centre of Excellence in Low Temperature Quantum Phenomena and Devices No. 284594).

References and Notes

- [1] De Feyter, S. *et al.* Two-dimensional supramolecular self-assembly probed by scanning tunneling microscopy. *Chemical Society Reviews* **32**, 139–150 (2003).
- [2] Slater, A. G. *et al.* Two-dimensional supramolecular chemistry on surfaces. *Chemical Science* **2**, 1440–1448 (2011).
- [3] Kudernac, T. *et al.* Two-dimensional supramolecular self-assembly: nanoporous networks on surfaces. *Chemical Society Reviews* **38**, 402–421 (2009).
- [4] Rosei, F. *et al.* Properties of large organic molecules on metal surfaces. *Progress in Surface Science* **71**, 95–146 (2003).
- [5] Matena, M. *et al.* On-surface synthesis of a two-dimensional porous coordination network: Unraveling adsorbate interactions. *Phys. Rev. B* **90**, 125408– (2014).
- [6] Grobis, M. *et al.* Local electronic properties of a molecular monolayer: c_{60} on $ag(001)$. *Phys. Rev. B* **66**, 161408– (2002).
- [7] Bedwani, S. *et al.* Strongly reshaped organic-metal interfaces: Tetracyanoethylene on $cu(100)$. *Physical Review Letters* **101**, 216105– (2008).
- [8] Fiori, G. *et al.* Electronics based on two-dimensional materials. *Nature nanotechnology* **9**, 768–779 (2014).
- [9] Mas-Balleste, R. *et al.* 2d materials: to graphene and beyond. *Nanoscale* **3**, 20–30 (2011).
- [10] Das, S. *et al.* Beyond graphene: Progress in novel two-dimensional materials and van der waals solids. *Annual Review of Materials Research* **45**, 1–27 (2015).
- [11] Neto, A. C. *et al.* The electronic properties of graphene. *Reviews of modern physics* **81**, 109 (2009).
- [12] Pakdel, A. *et al.* Nano boron nitride flatland. *Chemical Society Reviews* **43**, 934–959 (2014).
- [13] Wang, Q. H. *et al.* Electronics and optoelectronics of two-dimensional transition metal dichalcogenides. *Nature nanotechnology* **7**, 699–712 (2012).
- [14] Gupta, A. *et al.* Recent development in 2d materials beyond graphene. *Progress in Materials Science* **73**, 44–126 (2015).
- [15] Geim, A. K. Graphene: Status and prospects. *Science* **324**, 1530–1534 (2009).
- [16] Johns, J. E. *et al.* Atomic covalent functionalization of graphene. *Accounts of Chemical Research* **46**, 77–86 (2013).
- [17] Elias, D. C. *et al.* Control of graphene’s properties by reversible hydrogenation: Evidence for graphane. *Science* **323**, 610–613 (2009).
- [18] Balog, R. *et al.* Bandgap opening in graphene induced by patterned hydrogen adsorption. *Nature Materials* **9**, 315–319 (2010).

- [19] Ryder, C. R. *et al.* Chemically tailoring semiconducting two-dimensional transition metal dichalcogenides and black phosphorus. *ACS Nano* **10**, 3900–3917 (2016).
- [20] MacLeod, J. *et al.* Molecular self-assembly on graphene. *Small* **10**, 1038–1049 (2014).
- [21] Mali, K. S. *et al.* Nanostructuring graphene for controlled and reproducible functionalization. *Nanoscale* **7**, 1566–1585 (2015).
- [22] Liu, H. *et al.* Chemical doping of graphene. *Journal of materials chemistry* **21**, 3335–3345 (2011).
- [23] Zhang, Z. *et al.* Tailoring electronic properties of graphene by π – π stacking with aromatic molecules. *The Journal of Physical Chemistry Letters* **2**, 2897–2905 (2011).
- [24] Mao, H. Y. *et al.* Manipulating the electronic and chemical properties of graphene via molecular functionalization. *Progress in Surface Science* **88**, 132–159 (2013).
- [25] Tang, Q. *et al.* Graphene-related nanomaterials: tuning properties by functionalization. *Nanoscale* **5**, 4541–4583 (2013).
- [26] Kong, L. *et al.* Molecular adsorption on graphene. *Journal of Physics: Condensed Matter* **26**, 443001 (2014).
- [27] Georgakilas, V. *et al.* Functionalization of graphene: Covalent and non-covalent approaches, derivatives and applications. *Chemical Reviews* **112**, 6156–6214 (2012).
- [28] Koehler, F. M. *et al.* Organic synthesis on graphene. *Accounts of Chemical Research* **46**, 2297–2306 (2013).
- [29] Chua, C. K. *et al.* Covalent chemistry on graphene. *Chemical Society Reviews* **42**, 3222–3233 (2013).
- [30] Voiry, D. *et al.* Covalent functionalization of monolayered transition metal dichalcogenides by phase engineering. *Nat. Chem.* **7**, 45–49 (2015).
- [31] Wang, H. *et al.* Physical and chemical tuning of two-dimensional transition metal dichalcogenides. *Chemical Society Reviews* **44**, 2664–2680 (2015).
- [32] Cai, B. *et al.* Noncovalent molecular doping of two-dimensional materials. *ChemNanoMat* **1**, 542–557 (2015).
- [33] Bonaccorso, F. *et al.* Production and processing of graphene and 2d crystals. *Materials Today* **15**, 564–589 (2012).
- [34] Dean, C. R. *et al.* Boron nitride substrates for high-quality graphene electronics. *Nat. Nano.* **5**, 722–726 (2010).
- [35] Yankowitz, M. *et al.* Graphene on hexagonal boron nitride. *Journal of Physics: Condensed Matter* **26**, 303201 (2014).
- [36] Norimatsu, W. *et al.* Epitaxial graphene on sic {0001}: advances and perspectives. *Physical Chemistry Chemical Physics* **16**, 3501–3511 (2014).

- [37] Batzill, M. The surface science of graphene: Metal interfaces, cvd synthesis, nanoribbons, chemical modifications, and defects. *Surface Science Reports* **67**, 83–115 (2012).
- [38] Yang, W. *et al.* Epitaxial growth of single-domain graphene on hexagonal boron nitride. *Nature Materials* **12**, 792–797 (2013).
- [39] Varchon, F. *et al.* Electronic structure of epitaxial graphene layers on sic: effect of the substrate. *Physical review letters* **99**, 126805 (2007).
- [40] Ohta, T. *et al.* Interlayer interaction and electronic screening in multilayer graphene investigated with angle-resolved photoemission spectroscopy. *Physical Review Letters* **98**, 206802 (2007).
- [41] Wintterlin, J. *et al.* Graphene on metal surfaces. *Surface Science* **603**, 1841–1852 (2009).
- [42] Pletikoscic, I. *et al.* Dirac cones and minigaps for graphene on ir(111). *Physical Review Letters* **102**, 056808 (2009).
- [43] Sutter, P. *et al.* Graphene on pt(111): Growth and substrate interaction. *Phys. Rev. B* **80**, 245411 (2009).
- [44] Busse, C. *et al.* Graphene on ir(111): Physisorption with chemical modulation. *Physical Review Letters* **107**, 036101 (2011).
- [45] Hämäläinen, S. K. *et al.* Structure and local variations of the graphene moiré on ir(111). *Phys. Rev. B* **88**, 201406 (2013).
- [46] Moritz, W. *et al.* Structure determination of the coincidence phase of graphene on ru(0001). *Physical Review Letters* **104**, 136102 (2010).
- [47] Wang, B. *et al.* Coupling epitaxy, chemical bonding, and work function at the local scale in transition metal-supported graphene. *Acs Nano* **4**, 5773–5782 (2010).
- [48] Auwärter, W. *et al.* Defect lines and two-domain structure of hexagonal boron nitride films on ni(111). *Surface Science* **545**, L735–L740 (2003).
- [49] Dahal, A. *et al.* Graphene-nickel interfaces: a review. *Nanoscale* **6**, 2548–2562 (2014).
- [50] Drost, R. *et al.* Synthesis of extended atomically perfect zigzag graphene - boron nitride interfaces. *Sci. Rep.* **5**, 16741 (2015).
- [51] Voloshina, E. *et al.* Graphene on metallic surfaces: problems and perspectives. *Physical Chemistry Chemical Physics* **14**, 13502–13514 (2012).
- [52] Schulz, F. *et al.* Epitaxial hexagonal boron nitride on ir(111): A work function template. *Phys. Rev. B* **89**, 235429 (2014).
- [53] Díaz, J. G. *et al.* Hexagonal boron nitride on transition metal surfaces. *Theoretical Chemistry Accounts* **132**, 1–17 (2013).
- [54] Corso, M. *et al.* Boron nitride nanomesh. *Science* **303**, 217–220 (2004).

- [55] Brugger, T. *et al.* Comparison of electronic structure and template function of single-layer graphene and a hexagonal boron nitride nanomesh on ru (0001). *Physical Review B* **79**, 045407 (2009).
- [56] Cavar, E. *et al.* A single h-bn layer on pt (111). *Surface Science* **602**, 1722–1726 (2008).
- [57] Joshi, S. *et al.* Boron nitride on cu(111): An electronically corrugated monolayer. *Nano Letters* **12**, 5821–5828 (2012).
- [58] Goriachko, A. *et al.* Self-assembly of a hexagonal boron nitride nanomesh on ru (0001). *Langmuir* **23**, 2928–2931 (2007).
- [59] Dil, H. *et al.* Surface trapping of atoms and molecules with dipole rings. *Science* **319**, 1824 (2008).
- [60] Mao, J. *et al.* Tunability of supramolecular kagome lattices of magnetic phthalocyanines using graphene-based moire patterns as templates. *Journal of the American Chemical Society* **131**, 1413614137 (2009).
- [61] Yang, K. *et al.* Molecule substrate coupling between metal phthalocyanines and epitaxial graphene grown on ru(0001) and pt(111). *Journal of Physical Chemistry C* **116**, 1405214056 (2012).
- [62] Zhang, H. G. *et al.* Assembly of iron phthalocyanine and pentacene molecules on a graphene monolayer grown on ru(0001). *Phys. Rev. B* **84**, 245436 (2011).
- [63] Zhang, H. *et al.* Host guest superstructures on graphene-based kagome lattice. *Journal of Physical Chemistry C* **116**, 1109111095 (2012).
- [64] Zhou, H. *et al.* Template-directed assembly of pentacene molecules on epitaxial graphene on ru (0001). *Nano Research* **6**, 131–137 (2013).
- [65] Roos, M. *et al.* Intermolecular vs molecule–substrate interactions: A combined stm and theoretical study of supramolecular phases on graphene/ru (0001). *Beilstein journal of nanotechnology* **2**, 365–373 (2011).
- [66] Zhou, H. T. *et al.* Direct imaging of intrinsic molecular orbitals using two-dimensional, epitaxially-grown, nanostructured graphene for study of single molecule and interactions. *Applied Physics Letters* **99**, 153101 (2011).
- [67] Garnica, M. *et al.* Long-range magnetic order in a purely organic 2d layer adsorbed on epitaxial graphene. *Nature Physics* **9**, 368 (2013).
- [68] Maccariello, D. *et al.* Spatially resolved, site-dependent charge transfer and induced magnetic moment in tcnq adsorbed on graphene. *Chemistry of Materials* **26**, 28832890 (2014).
- [69] Lu, J. *et al.* Using the graphene moiré pattern for the trapping of c60 and homoepitaxy of graphene. *Acs Nano* **6**, 944 (2012).
- [70] Li, G. *et al.* Self-assembly of c60 monolayer on epitaxially grown, nanostructured graphene on ru (0001) surface. *Applied Physics Letters* **100**, 013304 (2012).

- [71] Järvinen, P. *et al.* Self-assembly and orbital imaging of metal phthalocyanines on a graphene model surface. *J. Phys. Chem. C* **118**, 13320–13325 (2014).
- [72] Tsai, H.-Z. *et al.* Molecular self-assembly in a poorly screened environment: F4tcnq on graphene/bn. *ACS nano* **9**, 12168–12173 (2015).
- [73] Lin, X. *et al.* Self-assembly of mgpc molecules on polar feo thin films. *J. Phys. Chem. C* **112**, 15325–15328 (2008).
- [74] Milian, B. *et al.* On the electron affinity of tcnq. *Chemical Physics Letters* **391**, 148–151 (2004).
- [75] Iannuzzi, M. *et al.* Site-selective adsorption of phthalocyanine on h-bn/rh(111) nanomesh. *Physical Chemistry Chemical Physics* **16**, 12374 (2014).
- [76] Schulz, F. *et al.* Templated self-assembly and local doping of molecules on epitaxial hexagonal boron nitride. *ACS nano* **7**, 11121–11128 (2013).
- [77] Joshi, S. *et al.* Control of molecular organization and energy level alignment by an electronically nanopatterned boron nitride template. *Acs Nano* **8**, 430 (2014).
- [78] Berner, S. *et al.* Boron nitride nanomesh: Functionality from a corrugated monolayer. *Angewandte Chemie International Edition* **46**, 5115–5119 (2007).
- [79] Dienel, T. *et al.* Dehalogenation and coupling of a polycyclic hydrocarbon on an atomically thin insulator. *ACS Nano* **8**, 6571–6579 (2014).
- [80] Widmer, R. *et al.* Probing the selectivity of a nanostructured surface by xenon adsorption. *Nanoscale* **2**, 502–508 (2010).
- [81] Urgel, J. I. *et al.* Controlling coordination reactions and assembly on a cu(111) supported boron nitride monolayer. *Journal of the American Chemical Society* **137**, 2420–2423 (2015).
- [82] Dedkov, Y. *et al.* Multichannel scanning probe microscopy and spectroscopy of graphene moire structures. *Physical Chemistry Chemical Physics* **16**, 3894–3908 (2014).
- [83] Altenburg, S. J. *et al.* Local work function and stm tip-induced distortion of graphene on ir(111). *New Journal of Physics* **16**, 053036 (2014).
- [84] Sun, Z. *et al.* Topographic and electronic contrast of the graphene moiré on ir(111) probed by scanning tunneling microscopy and noncontact atomic force microscopy. *Phys. Rev. B* **83**, 081415 (2011).
- [85] Barja, S. *et al.* Self-organization of electron acceptor molecules on graphene. *Chemical Communications* **46**, 8198 (2010).
- [86] Hamalainen, S. K. *et al.* Self-assembly of cobalt-phthalocyanine molecules on epitaxial graphene on ir(111). *J. Phys. Chem. C* **116**, 20433 (2012).
- [87] Wang, Y.-L. *et al.* Selective adsorption and electronic interaction of f16cupc on epitaxial graphene. *Physical Review B* **82**, 245420 (2010).

- [88] Järvinen, P. *et al.* Molecular self-assembly on graphene on SiO_2 and h-BN substrates. *Nano Letters* **13**, 3199 (2013).
- [89] Jung, M. *et al.* Atomically resolved orientational ordering of C₆₀ molecules on epitaxial graphene on Cu(111). *Nanoscale* **6**, 11835–11840 (2014).
- [90] Cho, J. *et al.* Structural and electronic decoupling of C₆₀ from epitaxial graphene on SiC. *Nano Letters* **12**, 3018–3024 (2012).
- [91] Švec, M. *et al.* van der Waals interactions mediating the cohesion of fullerenes on graphene. *Physical Review B* **86**, 121407 (2012).
- [92] Martínez-Galera, A. J. *et al.* Imaging molecular orbitals of PTCDA on graphene on Pt(111): Electronic structure by STM and first-principles calculations. *J. Phys. Chem. C* **118**, 12782 (2014).
- [93] Huang, H. *et al.* Structural and electronic properties of PTCDA thin films on epitaxial graphene. *ACS nano* **3**, 3431–3436 (2009).
- [94] Wang, Q. H. *et al.* Room-temperature molecular-resolution characterization of self-assembled organic monolayers on epitaxial graphene. *Nature Chemistry* **1**, 206–211 (2009).
- [95] Emery, J. D. *et al.* Structural analysis of PTCDA monolayers on epitaxial graphene with ultra-high vacuum scanning tunneling microscopy and high-resolution x-ray reflectivity. *Surface Science* **605**, 1685–1693 (2011).
- [96] Alaboson, J. M. *et al.* Seeding atomic layer deposition of high-k dielectrics on epitaxial graphene with organic self-assembled monolayers. *ACS nano* **5**, 5223–5232 (2011).
- [97] Karmel, H. J. *et al.* Self-assembled organic monolayers on epitaxial graphene with enhanced structural and thermal stability. *Chemical Communications* **50**, 8852–8855 (2014).
- [98] Stradi, D. *et al.* Controlling the spatial arrangement of organic magnetic anions adsorbed on epitaxial graphene on Ru(0001). *Nanoscale* **6**, 15271 (2014).
- [99] Decker, R. *et al.* Atomic-scale magnetism of cobalt-intercalated graphene. *Phys. Rev. B* **87**, 041403 (2013).
- [100] Decker, R. *et al.* Local tunnel magnetoresistance of an iron intercalated graphene-based heterostructure. *Journal of Physics: Condensed Matter* **26**, 394004 (2014).
- [101] Bazarnik, M. *et al.* Tailoring molecular self-assembly of magnetic phthalocyanine molecules on Fe- and Co-intercalated graphene. *ACS Nano* **12**, 11341 (2013).
- [102] Roos, M. *et al.* Hierarchical interactions and their influence upon the adsorption of organic molecules on a graphene film. *Journal of the American Chemical Society* **133**, 9208–9211 (2011).
- [103] Zhou, Q. *et al.* Switchable supramolecular assemblies on graphene. *Nanoscale* **6**, 8387–8391 (2014).
- [104] Banerjee, K. *et al.* Flexible self-assembled molecular templates on graphene. *The Journal of Physical Chemistry C* **120**, 8772–8780 (2016).

- [105] Jung, W. *et al.* Influence of graphene-substrate interactions on configurations of organic molecules on graphene: Pentacene/epitaxial graphene/sic. *Applied Physics Letters* **105**, 071606 (2014).
- [106] Chen, W. *et al.* Molecular orientation transition of organic thin films on graphite: the effect of intermolecular electrostatic and interfacial dispersion forces. *Chemical Communications* 4276–4278 (2008).
- [107] Karmel, H. J. *et al.* Self-assembled two-dimensional heteromolecular nanoporous molecular arrays on epitaxial graphene. *The Journal of Physical Chemistry Letters* **5**, 270–274 (2013).
- [108] Lackinger, M. *et al.* Carboxylic acids: Versatile building blocks and mediators for two-dimensional supramolecular self-assembly. *Langmuir* **25**, 11307–11321 (2009).
- [109] MacLeod, J. *et al.* Substrate effects in the supramolecular assembly of 1, 3, 5-benzene tricarboxylic acid on graphite and graphene. *Langmuir* **31**, 7016–7024 (2015).
- [110] Xi, M. *et al.* Iodobenzene on cu(111): formation and coupling of adsorbed phenyl groups. *Surface Science* **278**, 19 – 32 (1992).
- [111] Hla, S.-W. *et al.* Inducing all steps of a chemical reaction with the scanning tunneling microscope tip: Towards single molecule engineering. *Physical Review Letters* **85**, 2777–2780 (2000).
- [112] Grill, L. *et al.* Nano-architectures by covalent assembly of molecular building blocks. *Nat. Nano.* **2**, 687–691 (2007).
- [113] Cai, J. *et al.* Atomically precise bottom-up fabrication of graphene nanoribbons. *Nature* **466**, 470–473 (2010).
- [114] Lafferentz, L. *et al.* Conductance of a single conjugated polymer as a continuous function of its length. *Science* **323**, 1193–1197 (2009).
- [115] Chen, Y.-C. *et al.* Tuning the band gap of graphene nanoribbons synthesized from molecular precursors. *ACS Nano* **7**, 6123–6128 (2013).
- [116] Cai, J. *et al.* Graphene nanoribbon heterojunctions. *Nat. Nano.* **9**, 896–900 (2014).
- [117] Kimouche, A. *et al.* Ultra-narrow metallic armchair graphene nanoribbons. *Nat. Commun.* **6**, 10177 (2015).
- [118] Chen, Y.-C. *et al.* Molecular bandgap engineering of bottom-up synthesized graphene nanoribbon heterojunctions. *Nat. Nano.* **10**, 156–160 (2015).
- [119] Ruffieux, P. *et al.* On-surface synthesis of graphene nanoribbons with zigzag edge topology. *Nature* **531**, 489–492 (2016).
- [120] Talirz, L. *et al.* On-surface synthesis of atomically precise graphene nanoribbons. *Advanced Materials* **28**, 6222–6231 (2016).
- [121] Bieri, M. *et al.* Two-dimensional polymer formation on surfaces: Insight into the roles of precursor mobility and reactivity. *Journal of the American Chemical Society* **132**, 16669–16676 (2010).

- [122] Bacle, P. *et al.* Chemical reactions on metal-supported hexagonal boron nitride investigated with density functional theory. *Chimia* **68**, 596–601 (2014-09-24T00:00:00).
- [123] Morchutt, C. *et al.* Covalent coupling via dehalogenation on ni(111) supported boron nitride and graphene. *Chemical Communications* **51**, 2440–2443 (2015).
- [124] Néel, N. *et al.* Depopulation of single-phthalocyanine molecular orbitals upon pyrrolic-hydrogen abstraction on graphene. *ACS Nano* **10**, 2010–2016 (2016).
- [125] Altenburg, S. J. *et al.* Reaction of phthalocyanines with graphene on ir(111). *Journal of the American Chemical Society* **137**, 9452–9458 (2015).
- [126] Norskov, J. K. *et al.* Density functional theory in surface chemistry and catalysis. *Proceedings of the National Academy of Sciences* **108**, 937–943 (2011).
- [127] Nilsson, A. *et al.* Chemical bonding on surfaces probed by x-ray emission spectroscopy and density functional theory. *Surface Science Reports* **55**, 49–167 (2004).
- [128] Chavy, C. *et al.* Interpretation of stm images: C60 on the gold (110) surface. *Chemical Physics Letters* **214**, 569–575 (1993).
- [129] Repp, J. *et al.* Molecules on insulating films: Scanning-tunneling microscopy imaging of individual molecular orbitals. *Physical Review Letters* **94**, 026803 (2005).
- [130] Repp, J. *et al.* Imaging bond formation between a gold atom and pentacene on an insulating surface. *Science* **312**, 1196–1199 (2006).
- [131] Liljeroth, P. *et al.* Current-induced hydrogen tautomerization and conductance switching of naphthalocyanine molecules. *Science* **317**, 1203 (2007).
- [132] Qiu, X. H. *et al.* Vibrationally resolved fluorescence excited with submolecular precision. *Science* **299**, 542–546 (2003).
- [133] Liu, N. *et al.* Vibronic states in single molecules: C60 and c70 on ultrathin al₂o₃ films. *Journal of Chemical Physics* **120**, 11371 (2004).
- [134] Tsukahara, N. *et al.* Adsorption-induced switching of magnetic anisotropy in a single iron(ii) phthalocyanine molecule on an oxidized cu(110) surface. *Physical Review Letters* **102**, 167203 (2009).
- [135] Hirjibehedin, C. F. *et al.* Large magnetic anisotropy of a single atomic spin embedded in a surface molecular network. *Science* **317**, 1199–1203 (2007).
- [136] Zoldan, V. C. *et al.* Coupling of cobalt-tetraphenylporphyrin molecules to a copper nitride layer. *J. Phys. Chem. C* **117**, 15984–15990 (2013).
- [137] Bellec, A. *et al.* Imaging molecular orbitals by scanning tunneling microscopy on a passivated semiconductor. *Nano Letters* **9**, 144–147 (2009).
- [138] Godlewski, S. *et al.* Contacting a conjugated molecule with a surface dangling bond dimer on a hydrogenated ge(001) surface allows imaging of the hidden ground electronic state. *ACS Nano* **7**, 10105–10111 (2013).

- [139] Kahle, S. *et al.* The quantum magnetism of individual manganese-12-acetate molecular magnets anchored at surfaces. *Nano Letters* **12**, 518–521 (2012).
- [140] Swart, I. *et al.* Single-molecule chemistry and physics explored by low-temperature scanning probe microscopy. *Chemical Communications* **47**, 9011–9023 (2011).
- [141] Hill, I. *et al.* Charge-separation energy in films of π -conjugated organic molecules. *Chemical Physics Letters* **327**, 181–188 (2000).
- [142] van der Molen, S. J. *et al.* Charge transport through molecular switches. *Journal of Physics: Condensed Matter* **22**, 133001 (2010).
- [143] Ishii, H. *et al.* Energy level alignment and interfacial electronic structures at organic/metal and organic/organic interfaces. *Adv. Mater.* **11**, 605–625 (1999).
- [144] Tsiper, E. *et al.* Electronic polarization at surfaces and thin films of organic molecular crystals: Ptcda. *Chemical Physics Letters* **360**, 47–52 (2002).
- [145] Neaton, J. B. *et al.* Renormalization of molecular electronic levels at metal-molecule interfaces. *Physical Review Letters* **97**, 216405– (2006).
- [146] Braun, S. *et al.* Energy-level alignment at organic/metal and organic/organic interfaces. *Adv. Mater.* **21**, 1450–1472 (2009).
- [147] Gross, L. *et al.* High-resolution molecular orbital imaging using a p -wave stm tip. *Physical Review Letters* **107**, 086101 (2011).
- [148] Endlich, M. *et al.* Phthalocyanine adsorption to graphene on ir(111): Evidence for decoupling from vibrational spectroscopy. *The Journal of Chemical Physics* **141**, 184308 (2014).
- [149] Zheng, Y. J. *et al.* Heterointerface screening effects between organic monolayers and monolayer transition metal dichalcogenides. *ACS nano* **10**, 2476–2484 (2016).
- [150] Lu, X. *et al.* Charge transfer and screening in individual c_{60} molecules on metal substrates: A scanning tunneling spectroscopy and theoretical study. *Phys. Rev. B* **70**, 115418– (2004).
- [151] Scardamaglia, M. *et al.* Metal-phthalocyanine array on the moiré pattern of a graphene sheet. *Journal of Nanoparticle Research* **13**, 6013–6020 (2011).
- [152] Scardamaglia, M. *et al.* Energetics and hierarchical interactions of metal-phthalocyanines adsorbed on graphene/ir (111). *Langmuir* **29**, 10440–10447 (2013).
- [153] Dou, W. *et al.* Molecule-substrate interaction channels of metal-phthalocyanines on graphene on ni (111) surface. *The Journal of chemical physics* **134**, 094705 (2011).
- [154] Riss, A. *et al.* Imaging and tuning molecular levels at the surface of a gated graphene device. *ACS nano* **8**, 5395–5401 (2014).
- [155] Schulz, F. *et al.* Many-body transitions in a single molecule visualized by scanning tunnelling microscopy. *Nature Physics* **11**, 229–234 (2015).

- [156] Liu, L. *et al.* Interplay between energy-level position and charging effect of manganese phthalocyanines on an atomically thin insulator. *ACS Nano* **9**, 10125–10132 (2015).
- [157] Nazin, G. *et al.* Tunneling rates in electron transport through double-barrier molecular junctions in a scanning tunneling microscope. *Proceedings of the National Academy of Sciences of the United States of America* **102**, 8832–8837 (2005).
- [158] Repp, J. *et al.* Coherent electron-nuclear coupling in oligothiophene molecular wires. *Nature Physics* **6**, 975–979 (2010).
- [159] Wingreen, N. S. *et al.* Inelastic scattering in resonant tunneling. *Physical Review B* **40**, 11834 (1989).
- [160] Gadzuk, J. Inelastic resonance scattering, tunneling, and desorption. *Physical Review B* **44**, 13466 (1991).
- [161] Galperin, M. *et al.* Molecular transport junctions: vibrational effects. *Journal of Physics: Condensed Matter* **19**, 103201 (2007).
- [162] Pradhan, N. A. *et al.* Atomic scale conductance induced by single impurity charging. *Physical Review Letters* **94**, 076801– (2005).
- [163] Marczinowski, F. *et al.* Effect of charge manipulation on scanning tunneling spectra of single mn acceptors in inas. *Phys. Rev. B* **77**, 115318– (2008).
- [164] Sarma, S. D. *et al.* Electronic transport in two-dimensional graphene. *Reviews of Modern Physics* **83**, 407 (2011).
- [165] Schwierz, F. Graphene transistors. *Nature nanotechnology* **5**, 487–496 (2010).
- [166] Li, X. *et al.* Chemically derived, ultrasmooth graphene nanoribbon semiconductors. *Science* **319**, 1229–1232 (2008).
- [167] Han, M. Y. *et al.* Energy band-gap engineering of graphene nanoribbons. *Physical review letters* **98**, 206805 (2007).
- [168] Eroms, J. *et al.* Weak localization and transport gap in graphene antidot lattices. *New Journal of Physics* **11**, 095021 (2009).
- [169] Giesbers, A. *et al.* Charge transport gap in graphene antidot lattices. *Physical Review B* **86**, 045445 (2012).
- [170] Kosynkin, D. V. *et al.* Longitudinal unzipping of carbon nanotubes to form graphene nanoribbons. *Nature* **458**, 872–876 (2009).
- [171] Tao, C. *et al.* Spatially resolving edge states of chiral graphene nanoribbons. *Nature Physics* **7**, 616–620 (2011).
- [172] Llinas, J. P. *et al.* Short-channel field effect transistors with 9-atom and 13-atom wide graphene nanoribbons. *arXiv preprint arXiv:1605.06730* (2016).
- [173] Hunt, B. *et al.* Massive dirac fermions and hofstadter butterfly in a van der waals heterostructure. *Science* **340**, 1427–1430 (2013).

- [174] Woods, C. *et al.* Commensurate-incommensurate transition in graphene on hexagonal boron nitride. *Nature physics* **10**, 451–456 (2014).
- [175] Nair, R. R. *et al.* Fluorographene: A two-dimensional counterpart of teflon. *Small* **6**, 2877–2884 (2010).
- [176] Panchakarla, L. *et al.* Synthesis, structure, and properties of boron-and nitrogen-doped graphene. *Advanced Materials* **21**, 4726 (2009).
- [177] Wei, D. *et al.* Synthesis of n-doped graphene by chemical vapor deposition and its electrical properties. *Nano letters* **9**, 1752–1758 (2009).
- [178] Telychko, M. *et al.* Achieving high-quality single-atom nitrogen doping of graphene/sic (0001) by ion implantation and subsequent thermal stabilization. *ACS nano* **8**, 7318–7324 (2014).
- [179] Sforzini, J. *et al.* Structural and electronic properties of nitrogen-doped graphene. *Physical review letters* **116**, 126805 (2016).
- [180] Sque, S. J. *et al.* The transfer doping of graphite and graphene. *physica status solidi (a)* **204**, 3078–3084 (2007).
- [181] Wehling, T. *et al.* Molecular doping of graphene. *Nano letters* **8**, 173–177 (2008).
- [182] Rochefort, A. *et al.* Interaction of substituted aromatic compounds with graphene. *Langmuir* **25**, 210–215 (2008).
- [183] Hu, T. *et al.* Theoretical study of the interaction of electron donor and acceptor molecules with graphene. *The Journal of Physical Chemistry C* **117**, 2411–2420 (2013).
- [184] Park, C.-H. *et al.* New generation of massless dirac fermions in graphene under external periodic potentials. *Physical review letters* **101**, 126804 (2008).
- [185] Romero, H. E. *et al.* Adsorption of ammonia on graphene. *Nanotechnology* **20**, 245501 (2009).
- [186] Farmer, D. B. *et al.* Chemical doping and electron- hole conduction asymmetry in graphene devices. *Nano letters* **9**, 388–392 (2008).
- [187] Dong, X. *et al.* Doping single-layer graphene with aromatic molecules. *Small* **5**, 1422–1426 (2009).
- [188] Moser, J. *et al.* The environment of graphene probed by electrostatic force microscopy. *Applied Physics Letters* **92**, 123507 (2008).
- [189] Sato, Y. *et al.* Electrically controlled adsorption of oxygen in bilayer graphene devices. *Nano letters* **11**, 3468–3475 (2011).
- [190] Sun, J. *et al.* Linear tuning of charge carriers in graphene by organic molecules and charge-transfer complexes. *Physical Review B* **81**, 155403 (2010).
- [191] Prado, M. C. *et al.* Two-dimensional molecular crystals of phosphonic acids on graphene. *ACS Nano* **5**, 394–398 (2010).

- [192] Coletti, C. *et al.* Charge neutrality and band-gap tuning of epitaxial graphene on sic by molecular doping. *Phys. Rev. B* **81**, 235401 (2010).
- [193] Li, B. *et al.* Toward tunable doping in graphene fets by molecular self-assembled monolayers. *Nanoscale* **5**, 9640–9644 (2013).
- [194] Lauffer, P. *et al.* Molecular and electronic structure of ptcd a on bilayer graphene on sic (0001) studied with scanning tunneling microscopy. *Physica status solidi (b)* **245**, 2064–2067 (2008).
- [195] Meissner, M. *et al.* Highly ordered growth of ptcd a on epitaxial bilayer graphene. *Surface Science* **606**, 1709–1715 (2012).
- [196] Jee, H.-g. *et al.* Pentacene as protection layers of graphene on sic surfaces. *Applied Physics Letters* **95**, 093107 (2009).
- [197] Chen, W. *et al.* Surface transfer p-type doping of epitaxial graphene. *Journal of the American Chemical Society* **129**, 10418–10422 (2007).
- [198] Jnawali, G. *et al.* Observation of ground-and excited-state charge transfer at the c60/graphene interface. *ACS nano* **9**, 7175–7185 (2015).
- [199] Pinto, H. *et al.* p-type doping of graphene with f4-tcnq. *Journal of Physics: Condensed Matter* **21**, 402001 (2009).
- [200] Manna, A. K. *et al.* Tuning the electronic structure of graphene by molecular charge transfer: a computational study. *Chemistry–An Asian Journal* **4**, 855–860 (2009).
- [201] Kanai, K. *et al.* Determination of electron affinity of electron accepting molecules. *Applied Physics A* **95**, 309–313 (2009).
- [202] Choudhury, D. *et al.* Xps evidence for molecular charge-transfer doping of graphene. *Chemical Physics Letters* **497**, 66–69 (2010).
- [203] Wang, X. *et al.* Quantitative analysis of graphene doping by organic molecular charge transfer. *The Journal of Physical Chemistry C* **115**, 7596–7602 (2011).
- [204] Kim, N. W. *et al.* Infrared spectroscopy of large scale single layer graphene on self assembled organic monolayer. *Applied Physics Letters* **104**, 041904 (2014).
- [205] Lee, W. H. *et al.* Control of graphene field-effect transistors by interfacial hydrophobic self-assembled monolayers. *Advanced Materials* **23**, 3460–3464 (2011).
- [206] Park, J. *et al.* Work-function engineering of graphene electrodes by self-assembled monolayers for high-performance organic field-effect transistors. *The journal of physical chemistry letters* **2**, 841–845 (2011).
- [207] Yokota, K. *et al.* Carrier control of graphene driven by the proximity effect of functionalized self-assembled monolayers. *Nano letters* **11**, 3669–3675 (2011).
- [208] Yan, Z. *et al.* Controlled modulation of electronic properties of graphene by self-assembled monolayers on sio2 substrates. *ACS nano* **5**, 1535–1540 (2011).

- [209] Park, J. *et al.* Single-gate bandgap opening of bilayer graphene by dual molecular doping. *Advanced materials* **24**, 407–411 (2012).
- [210] Zhang, Y. *et al.* Direct observation of a widely tunable bandgap in bilayer graphene. *Nature* **459**, 820–823 (2009).